Engineering Failure Analysis 160 (2024) 108209

Contents lists available at ScienceDirect

Engineering Failure Analysis

journal homepage: www.elsevier.com/locate/engfailanal

Dynamic increase factors for progressive collapse analysis of steel structures considering column buckling

Luca Possidente [a,*], Fabio Freddi [a], Nicola Tondini [b]

[a] Dept. of Civil, Environmental & Geomatic Engineering, University College of London, London WC1E 6BT, UK
[b] Dept. of Civil, Environmental & Mechanical Engineering, University of Trento, Via Mesiano 77, Trento, Italy

ARTICLE INFO

Keywords:
Dynamic increase factor
Progressive collapse
Steel structures
Column buckling
Robustness

ABSTRACT

Progressive or disproportionate collapse of structures may have severe socio-economic consequences. Aiming at buildings that can withstand such events, one solution is to prevent or minimize the propagation of damage that may lead to progressive collapse by means of robust design strategies. As a typical approach to model progressive collapse and assess robustness, the Alternate Path Method (APM) allows for static analyses, in which the dynamic effects induced by a sudden column loss are taken into account by amplifying loads through a Dynamic Increase Factor. Current recommendations for Dynamic Increase Factors to be used within non-linear static analyses have mainly considered beam-type collapse, overlooking other failure mechanisms, *e.g.*, column buckling. The present paper investigates the dynamic effects of steel structures subjected to progressive collapse when buckling of columns is relevant. Five low- to high-rise case study building structures are considered together with three different column loss scenarios. A numerical procedure is introduced to evaluate the Dynamic Increase Factors considering two different Engineering Demand Parameters (EDPs), suited for describing beam- and column-type mechanisms, respectively. As Dynamic Increase Factors are typically assessed by increasing the loads on all the spans (DIF), a procedure was proposed for deriving factors that apply only on the spans above the removal (DIF*), consistently with UFC guidelines. The obtained DIF and DIF* are compared with the current literature and with values recommended in the UFC guidelines, highlighting the limits of current recommendations. Relevant considerations on the derived Dynamic Increase Factors and failure mechanisms involved are provided.

1. Introduction

The progressive collapse of a structure refers to the scenario where localized damage in individual elements propagates and eventually leads to the failure of the entire structure or a part of it [1]. Progressive collapse is typically triggered by accidental events such as fires, explosions, or impacts, which have a relatively low probability of occurrence. Nevertheless, the severity of the potential consequences has raised awareness about the importance of studying and addressing the issue related to progressive collapse. Indeed, disasters like the collapse of the Ronan Point Building (London, 1968), the Murrah Federal Building (Oklahoma City, 1995), the World Trade Center (New York, 2001), and recently of the Champlain Towers (Miami, 2021) have demonstrated the significant social and economic losses that can result from progressive collapse [2–5].

* Corresponding author.
E-mail address: l.possidente@ucl.ac.uk (L. Possidente).

https://doi.org/10.1016/j.engfailanal.2024.108209
Received 22 January 2024; Received in revised form 29 February 2024; Accepted 6 March 2024
Available online 7 March 2024

In response to these events and the growing recognition of risks associated with progressive collapse, researchers have extensively investigated the phenomenon, and, over the past few decades, substantial progress has been made in comprehending the mechanisms involved in progressive collapse for various structural systems [1,6]. By integrating lessons learned from past disasters and the advancements in progressive collapse research, design codes and standards [7–9] have been updated to provide guidance on mitigating the risks associated with this phenomenon. These codes aim to enhance the robustness and resilience of structures, ensuring they can withstand accidental events and prevent or minimize the propagation of damage that may lead to progressive collapse.

Several aspects related to progressive collapse mechanisms have been investigated in the last few decades, including system and components experimental tests [10–24], as well as numerical simulation [22–36]. Experimental tests allowed for increasing knowledge of specific phenomena and provided valuable data that can be used to inform and validate numerical models. These models are typically implemented for structural engineering applications by exploiting Finite Element (FE) methods. Several FE commercial or open-source software have been used to investigate progressive collapse [37–41], and various FE modeling strategies have been developed to deal with extreme events, *e.g.,* fires [42,43] and impacts [44], or efficiently account for load redistributions in progressive collapse [45]. This allowed extensive studies on the response of several structural typologies and configurations to such extreme events, including residential buildings, industrial facilities, and strategic structures [25,26,31–33,35,46–50].

In particular, to analyze and assess the capability of a structure to redistribute loads, a well-established numerical procedure, referred to as the Alternate Path Method (APM) [9], is often employed. This method allows examining how the structure redistributes the loads and identifies alternate load paths that can effectively carry the loads previously supported by failed elements. The APM involves conducting numerical simulations in which the structure is initially subjected to gravity loads, and subsequently, it is subject to the loss of a structural element. To limit the number of possible analyses, the APM typically focuses on the most critical scenarios (*i.e.,* most significant hazard or consequences - maximizing risk), which often involve the sudden loss of one or more columns at the ground floor [20,25–29,36,50]. This particular condition poses a significant threat to the entire system's stability, as the ground story columns play a fundamental role in providing vertical load support and structural integrity. Nevertheless, it is noteworthy that while the sudden loss of a ground story column is a crucial scenario, design codes and standards also encompass other potential triggers of progressive collapse, such as column removal in different locations or the loss of other critical elements [7–9].

The APM is commonly addressed through static analyses, wherein the dynamic effects are indirectly taken into account by increasing the static loads using a Dynamic Increase Factor. The dynamic increase factors provided in design codes for non-linear static analyses is typically calculated based on a ductile failure mode that involves the plastic rotation of structural elements, components, and connections. For instance, the UFC [7] provides dynamic increase factors for non-linear static analysis that vary with the ratio between the plastic rotation angle θ_{pra} defined according to the acceptance criteria [7] and yield rotation θ_y, which depend on the material and mechanical properties of the affected 'Deformation-Controlled' structural members only. However, it is noteworthy that, in some cases, the dynamic response of a structure during progressive collapse is not solely dependent on the deformation of the ductile components.

In fact, the response may be controlled by brittle collapse mechanisms or 'Force-Controlled' actions [7], such as column buckling in steel frames or shear failure in RC beams. In these situations, the UFC provides a dynamic increase factor specific for force-controlled actions only for elastic analysis, *i.e.,* 2. This value is very conservative, as it refers to the case of an undamped Single Degree of Freedom (SDoF) system [51]. Conversely, for non-linear static analyses, the UFC recommends the same dynamic increase factors derived for deformation-controlled actions. More detailed considerations involving brittle mechanisms are thus required to effectively evaluate the dynamic increase factors, given that different mechanisms might also induce different collapse modes, *e.g.,* pancake, domino, zipper, or mixed-type modes [52]. Column buckling, for example, is a phenomenon that can lead to brittle failure in steel structures and requires specific attention.

In recent decades, several studies have proposed alternative formulations for the dynamic increase factors [53–59], exploring different approaches to account for dynamic effects. Similarly to UFC [7], a ductility-based formulation was proposed by Stevens *et al.* [53], while a damping ratio was considered in Mashhadi and Saffari [54]. Various researchers worked in the direction of providing formulations for dynamic increase factors that depend on the actual structural state, for instance, by considering the ratio between the demand and capacity bending moment of the most stressed beam ends M_d/M_{pl} of the damaged structure under the original unamplified static gravity loads [55–57]. Tsai [58] presented two formulations for dynamic increase factors obtained for given displacements or load levels for an inelastic SDOF model. Ferraioli [59] proposed a modal pushdown procedure for progressive collapse analysis and estimation of dynamic increase factors of steel framed structures. Similarly, Brunesi and Parisi [60] assessed the dynamic effects in reinforced concrete framed structures in relation to the vertical displacement of beams based on pushdown analyses and Monte Carlo simulation. Only recently, Elsanadedy *et al.* [61] investigated the behavior of a multi-story frame steel building under single and multiple-column loss scenarios, including column initial imperfections, and evaluated the dynamic increase factors for linear static analyses. However, current literature lacks extensive investigation into the influence of the dynamic effects on the progressive collapse of structures experiencing brittle mechanisms, *e.g.,* steel structures prone to column buckling.

In this context, the present study evaluates the dynamic increase factors considering five steel Moment Resisting Frames (MRF) ranging from low- to high-rise structures and three different ground story column loss scenarios. The employed procedure enables the evaluation of different dynamic increase factors by considering Engineering Demand Parameters (EDPs) relevant to different collapse mechanisms. Detailed FE models were developed in OpenSees [37] for all the selected case-studies to perform non-linear static and dynamic analyses. The numerical models carefully considered global and local imperfections, and the response of key components was validated against experimental data and standard prescriptions to accurately simulate both beam and column-type mechanisms. The proposed analysis provided meaningful considerations about the dynamic effects and the dynamic increase factors, paying particular attention to the consistency and comparison with the current UFC [7] recommendations. Moreover, the paper presents a procedure for

deriving dynamic increase factors that apply only on the loads above the removal region (DIF*), as in UFC guidelines, from factors that apply to the loads on all spans (DIF). It is shown that the UFC suggests dynamic increase factors that are not capable of differentiating the dynamic contributions observed for structures with different characteristics and that may be subjected to column buckling.

The paper is organized as follows: Section 2 describes the case studies and the FE modeling strategy employed; Section 3 provides the methodology to assess the dynamic effects and determine the dynamic increase factors; Section 4 presents and discusses the results of preliminary analyses to characterize the case studies and the application of the methodology to the case studies; finally, Section 5 provides some conclusive remarks.

2. Case studies structures and numerical models

Numerical models of five steel structures were defined to investigate the influence of the dynamic effects considering different geometric characteristics and three column removal scenarios. Models were developed in OpenSees [37], combining the most suited elements to analyze the behavior of the structural joints and elements. The model's capability to capture the behavior of both beams and columns was assessed and validated.

2.1. Case studies description

Five case-study seismically designed MRFs with different numbers of stories were investigated. These MRFs were selected as benchmark case studies as they were already examined in previous research focusing on progressive collapse, and detailed information can be found in Gerasimidis *et al.* [48]. The seismic design was performed for a horizontal peak ground acceleration equal to 0.16 g and complying with the Eurocode recommendations [62–64]. Plane frames in the *x*-direction consisting of 4 bays with 5 m spans were analyzed, while the bay span in the other direction was considered 7 m for the definition of the loads. The frames have inter-story heights of 3 m and total heights of 9, 18, 27, 36, and 45 m, respectively, for the 3-, 6-, 9-, 12-, and 15-story structures. Fig. 1 shows the elevation views and the columns considered in the loss scenarios. Three single-column loss scenarios were defined, one for a perimeter and two for internal columns. The scenarios involving the remaining ground story columns were not considered due to symmetry conditions. The steel sections are oriented with the major axis within the frame plane, and beam-column joints were designed as rigid, full-strength welded joints. Nominal yield strength $f_y = 235$ MPa, Young's modulus $E = 210{,}000$ MPa, and Poisson ratio $\nu = 0.3$ were used. Table 1 summarizes the steel cross-sections for columns and beams.

A Dead Load (DL) equal to 5.0 kN/m^2 was applied on all floors, comprising 3.0 kN/m^2 of the self-weight of a 12 cm thick concrete slab and 2.0 kN/m^2 to account for the non-structural permanent components. An additional DL was applied directly to the structural elements to account for the self-weight of beams and columns. Except for the roof level, a Live Load (LL) of 2.00 kN/m^2 was applied on all floors. The Snow Load (SL) on the roof was assumed equal to 0.69 kN/m^2, based on Eurocode guidelines [62] for the Greek climate region in Zone III, 200 m of altitude and standard conditions. According to the UFC [7], the progressive collapse resistance is assessed by considering the following load combination:

$$q_d = 1.2\mathrm{DL} + 0.5\mathrm{LL} + 0.0\mathrm{SL} \tag{1}$$

The Work Ratio (WR) of the ground story columns when the structure is loaded under the load combination in Eq. (1) is reported in Table 1 and was calculated as the ratio between the axial force N and the buckling resistance about the weak axis $N_{z,bRd}$ according to EN1993-1-1 [63].

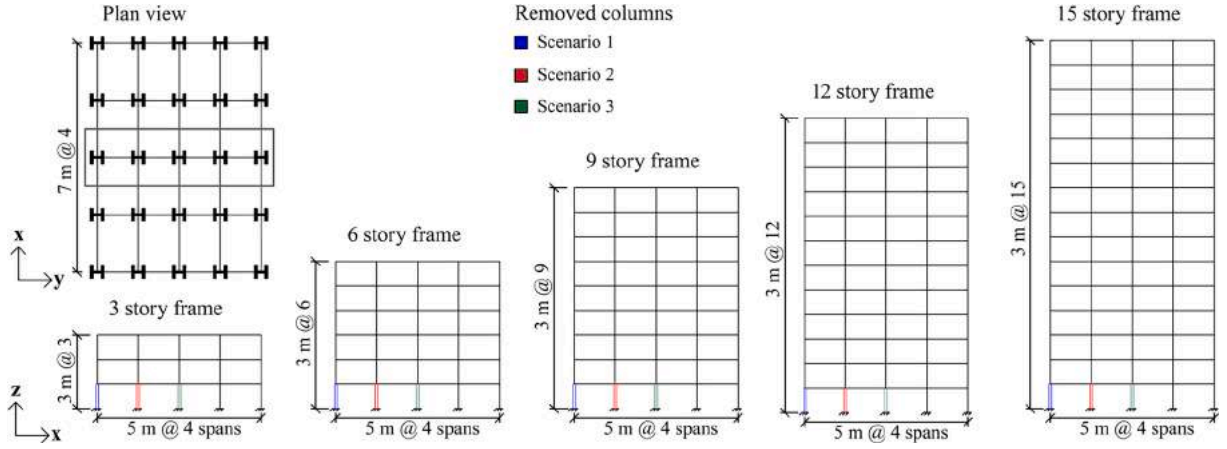

Fig. 1. Case studies MRFs and column loss scenarios. (Adapted from Gerasimidis et al. [48]).

Table 1
Case studies: columns and beam design. (Adapted from Gerasimidis et al. [48]).

N. of stories	Columns	Ground story columns Work Ratio (WR) [%]					Beams
		Col 1	Col 2	Col 3	Col 4	Col 5	
3	HE280B story 1 to 3	12.24	28.27	26.60	28.23	12.45	IPE500 story 1 IPE400 story 2 IPE360 story 3
6	HE320B story 1 to 3 HE220B story 4 to 6	20.63	45.55	44.12	45.46	21.20	IPE550 story 1 IPE450 story 2 to 3 IPE400 story 4 to 6 IPE360 story 6
9	HE400B story 1 to 3 HE280B story 4 to 6 HE220B story 7 to 9	25.98	53.02	53.43	52.91	26.87	IPE550 story 1 IPE500 story 2 to 3 IPE450 story 4 to 6 IPE400 story 7 to 8 IPE360 story 9
12	HE500B story 1 to 3 HE340B story 4 to 6 HE280B story 7 to 9 HE200B story 10 to 12	30.25	57.75	59.70	57.66	31.49	IPE550 story 1 IPE500 story 2 to 6 IPE450 story 7 to 9 IPE360 story 10 to 12
15	HE650B story 1 to 3 HE450B story 4 to 6 HE340B story 7 to 9 HE280B story 10 to 12 HE200B story 12 to 15	33.79	59.38	62.79	59.36	35.33	IPE550 story 1 to 2 IPE500 story 3 to 9 IPE450 story 10 to 12 IPE500 story 13 to 14 IPE450 story 15

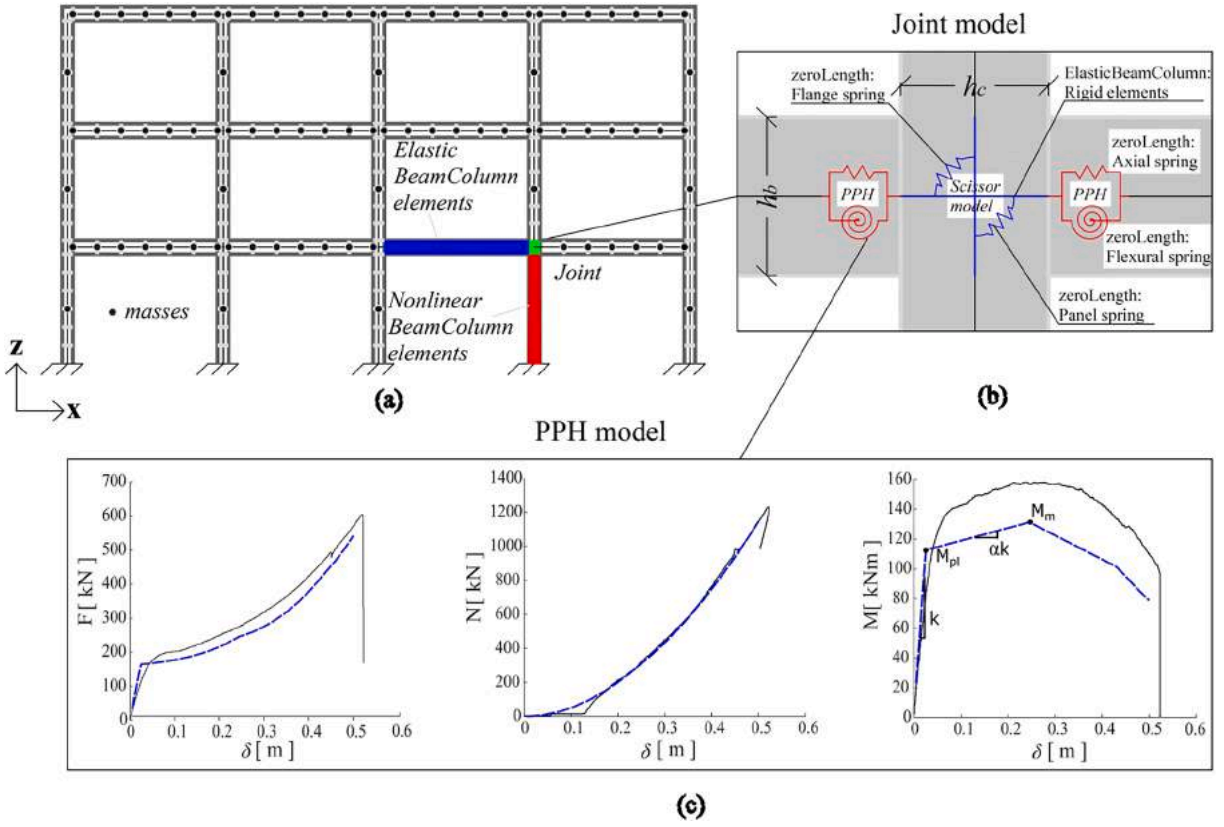

Fig. 2. Overview of the numerical modeling strategy.

2.2. Numerical models

The OpenSees software [37] was selected to define and investigate the numerical models of the five case studies owing to its modeling flexibility, which allowed for optimized use in terms of complexity and computational cost. The model complexity was increased only where needed, while simple and less computationally demanding features were employed elsewhere. In the latter case, additional analyses were performed to confirm that such simplifications were not influencing the obtained results.

Fig. 2 shows the key characteristics of the FE modeling strategy used in the present research work. Fiber elements were used for columns to exploit a distributed plasticity approach, and the elastic shear stiffness was included through the 'Section Aggregator' command. Ground story restraints were considered fixed in the *x*-direction and hinged in the *y*-direction. Additional lateral restraints were introduced at each floor to prevent a global out-of-plane loss of stability and account for the lateral stiffness of the slab.

To reduce the computational cost, the model discretization was optimized to have a reduced number of elements. Preliminary analyses showed that discretizing each column with 6 elements was sufficient to capture buckling (see Fig. 2(a)). Similarly, it was confirmed that using 33 concentrated masses at each story and 6 elements for each beam adequately discretized the problem to simulate the dynamic response adequately. A Rayleigh damping with a damping ratio $\xi = 5$ % was used in the simulation. The possible positive contribution of the slab to the progressive collapse resistance was conservatively neglected in the present study, and lateral-torsional buckling was not taken into account, considering the possible restraints provided by the slab.

Fig. 2(b) shows the modeling of the beam ends and the beam-column joint. A lumped plasticity approach was used for beams, considering plastic hinges at the beams' ends and implementing the 'Parallel Plastic Hinge' (PPH) model proposed by Lee *et al.* [68]. The PPH consists of two 'zeroLength' springs, with flexural and axial behavior, and allows capturing the bending moment and axial force interactions, typically observed in progressive collapse scenarios due to the large contribution provided by the catenary actions. Hence, the PPH model was connected to the elastic beam elements on one side and the rigid elements employed for the beam-column joint model on the other side. The panel zone deformation at beam-column joints was simulated using the 'Scissor Model' [69], whose main parameters were determined according to Charney and Downs [70]. The deformability of the column web panel and flanges is modeled through two independent flexural springs connected to two orthogonal rigid links whose extension is consistent with the physical dimensions of the nodes.

The PPH model was previously validated [36] against the experimental results presented by Dinu *et al.* [23]. As shown in Fig. 2(c), good agreement was found for the pushdown curve and the axial tension force, while the bending moment capacity was slightly underestimated. The evolution of the bending moment capacity reports the plastic-resisting bending moment of the steel beam (M_{pl}) and its maximum bending moment (M_m). Based on the calibration parameters, the same modeling strategy was implemented for the considered case-study structures.

The possible loss of stability and buckling effects were accounted for based on the EN1993-1-1 [63] recommendations. Global equivalent imperfections in terms of initial column rotation Φ were considered and both in-plane and out-of-plane local imperfections with a local magnitude e_o were introduced to account for the buckling of columns. Since particular attention was devoted to the behavior of the columns, the capability of the numerical model to account for buckling was carefully assessed. For this purpose, it was checked whether the EN1993-1-1 [63] buckling curves for compressed members could be obtained by means of numerical analysis, as depicted in Fig. 3. As shown in different applications [65,66], this goal can be achieved by introducing an imperfection consistent with the equation of the buckling load. Specifically, as also indicated in the ENV1993-1-1 [67], an initial imperfection with the following magnitude $e_{o,\eta}$ should be considered.

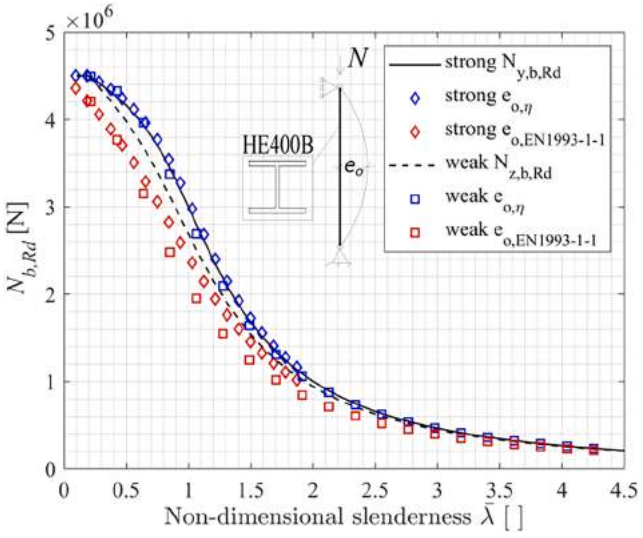

Fig. 3. Buckling model validation: strong and weak axis buckling curves.

$$e_{o,\eta} = k\eta = k\alpha(\bar{\lambda} - 0.2) \tag{2}$$

where $k = W_{el}/A$ is the kernel radius, defined as the ratio between the elastic section modulus W_{el} for the relevant axis and the area A of the section, η is the generalized imperfection factor, and α and $\bar{\lambda}$ are the imperfection factor and the non-dimensional slenderness according to EN1993-1-1 [63], respectively.

Simply supported axially loaded columns with HE400B section were investigated in OpenSees. When strong axis buckling was investigated, additional lateral restraints were introduced to avoid buckling on the weak axis. The same steel properties, *i.e.,* nominal yield strength $f_y = 235$ MPa and Young's modulus $E = 210{,}000$ MPa, distributed plasticity finite element, and discretization used for the columns of the case study structures were employed, considering an elastic-perfectly plastic stress–strain law to correctly capture both the buckling and yielding loads. In Fig. 3, the evolution of the axial force at failure with respect to the non-dimensional slenderness $\bar{\lambda}$ is compared to the EN1993-1-1 [63] buckling curves, showing a good agreement. For completeness, the analyses were also performed considering the magnitude of the local column imperfection $e_{o,EN1993\text{-}1\text{-}1}$ introduced in the numerical model of the case study structures, as currently prescribed in EN1993-1-1 [63]. It can be observed that more conservative results are obtained with this imperfection, and therefore, buckling is expected to initiate for loads lower than $N_{z,b,Rd}$ in the columns of the case studies.

3. Procedure for dynamic increase factor evaluation

A numerical procedure involving non-linear static and dynamic analyses to assess the dynamic effects of a sudden column loss scenario is presented. Such procedure is based on the APM [9] and allows for the numerical evaluation of the dynamic increase factors with respect to parameters relevant to beam- and column-type collapse mechanisms. To restore consistency between the factors obtained with the procedure and the recommendations provided in current standards as UFC [7], a transformation to obtain factors to increase only the loads above the removed columns is proposed.

3.1. Numerical procedure

The numerical procedure for the evaluation of dynamic increase factors consists of comparative analyses between response parameters of static and dynamic procedures.

The static response is obtained by performing pushdown analyses of the damaged structure, *i.e.,* the structure without the column (Fig. 4). In this procedure, the gravity loads are gradually increased in a non-linear quasi-static fashion until the structure is not able to carry any further load increment. To measure the capacity of the structure to withstand progressive collapse scenarios, the load factor λ is defined as follows:

$$\lambda = \frac{\sum_{i=1}^{n} R_i}{Q_{tg}} \tag{3}$$

where $\sum_{i=1}^{n} R_i$ is the sum of the n vertical ground story reaction forces of the frame and Q_{tg} is the load target the structure is supposed to bear according to a preselected load combination. According to this definition, the structure is not able to redistribute the load and, hence, is prone to progressive collapse if any failure is detected for $\lambda < 1$. Conversely, the structure has residual bearing capacity if failures occur for $\lambda > 1$.

On the other side, the dynamic response is examined by carrying out a three-step procedure aligned with the APM [9] and UFC [7] recommendations (Fig. 4). In Step 1, a static pushdown analysis is performed on the undamaged structure, *i.e.,* with no column removal, to determine the vertical ground story reaction R_c of the column to be removed. In Step 2, the damaged column is removed, and the state of the structure before removal is restored by gradually applying the gravity loads and a reaction force to the node above the removal. This force is the ground story reaction R_c, recorded in the gravity analysis in Step 1. Previous studies demonstrated that other forces, *e.g.,* shear forces and bending moments, do not significantly affect the final response and, thus, have been neglected [36]. In Step 3, a dynamic analysis is performed starting from the final state of Step 2 and applying a counterforce F_c to the node above removal to simulate the sudden column loss. The load has the same magnitude of R_c and is linearly applied within a short removal time T_{Rem}. T_{Rem} was taken as $(1/11)T_v$, according to GSA [9], which recommends employing $T_{Rem} < (1/10)T_v$, with T_v being the period corresponding to the first vertical vibration mode of the structure.

To compare the static and the dynamic responses, the dynamic analyses can be exploited in an Incremental Dynamic Analysis (IDA) fashion for increasing load values λ. This work considered ten analyses with constant increments of 10 % of the load factors. Notably, in each of these analyses, the mass varies accordingly with the load factor; therefore, the vibration periods and, in turn, the removal time

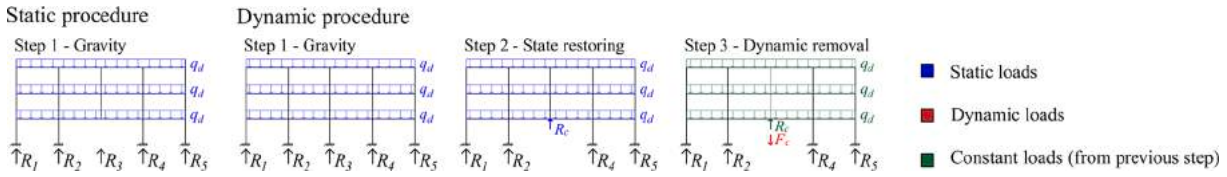

Fig. 4. Static and dynamic analyses for the evaluation of dynamic increase factors.

T_{Rem} vary.

3.2. Engineering demand parameters (EDPs)

The UFC [7] recommends checking all the relevant primary and secondary elements for deformation- and force-controlled actions. In this work, considering the possible failure mechanisms of the investigated MRFs, beams and columns subjected to deformation- and force-controlled actions, respectively, are identified as key elements. Hence, two different Engineering Demand Parameters (EDPs) are identified to evaluate the dynamic effects induced by one or more concurrent mechanisms while monitoring the performance of beams and columns, *i.e.,* the vertical displacement of the node above the removal δ and the axial compressive force in the columns adjacent to the removal N.

The displacement δ is proportional to the chord rotation, which is also typically used to monitor the performance of beams and is considered in the UFC [7] for the dynamic increase factors evaluation. On the other end, the axial force N is a 'good' indicator of buckling. The two dynamic increase factors, namely DIF, are derived from the numerical analyses according to a load-based approach, *i.e.,* measuring the ratio between the static and the dynamic load factors λ at the same EDP values:

$$\mathrm{DIF}_{\lambda}(\delta) = \frac{\lambda_S(\delta)}{\lambda_D(\delta)}; \qquad \mathrm{DIF}_{\lambda}(N) = \frac{\lambda_S(N)}{\lambda_D(N)} \tag{4}$$

where the subscripts D and S are related to the dynamic and static procedures.

In typical applications, the DIF is meant to increment the loads to account for dynamic effects and obtain the same response in static and dynamic analyses. Therefore, the load-based approach should be preferred to an EDP-based approach. Indeed, the load-based approach provides the load increment (λ_S/λ_D) necessary to obtain the desired effect in static analyses, *i.e.*, the same EDP values (δ_D or N_D) as in the dynamic one. Conversely, an EDP-based DIF cannot ensure the attainment of the same EDP values in the static and dynamic analyses. This approach implies that the DIF is determined as the ratio between dynamic and static EDPs (*e.g.,* δ_D/δ_S) at a given load factor, which stops being equivalent to the load-based DIF when the linear elastic range is overcome. Therefore, hereafter DIF will refer to load-based dynamic increase factors, though the presented procedure could also be employed to derive meaningful EDP-based DIFs, as shown in Freddi *et al.* [36].

3.3. Modified Dynamic Increase Factor (DIF*)

The dynamic increase factors obtained from the proposed procedure are evaluated by progressively increasing a uniform load applied on all spans. Therefore, to account for the dynamic effects in a static analysis, all gravity loads on all spans should be increased by such a factor. Conversely, following the recommendations of the UFC [7], the load must be amplified only on the bays above the removed column. Hence, to restore consistency between these two different amplifications of the gravity loads, a new dynamic increase factor, hereafter referred to as DIF*, is derived from the DIF obtained with the numerical procedure. The DIF* should be applied to any primary element, component, or connection in the model within or touching the area above the removed column, and its derivation is based on the static schemes in Fig. 5.

Fig. 5 describes three possible scenarios considering four equally long spans with length L and the same ground story columns, *i.e.,* same ground story restraint axial stiffness. This configuration was selected as equally long spans, and the same ground story columns are very common in structural design, and the contribution provided by additional spans farther from the collapse location is usually negligible [15]. Therefore, the considered schemes are suited to represent many structural applications with good approximation. Nevertheless, the derivation of the formulation for the DIF* can be based on other static schemes if necessary.

Three scenarios were studied by removing one of the ground story restraints and considering the two spans above internal column removal as a single span with a length 2L. The DIF* was derived for the relevant EDPs by enforcing the same vertical displacement v above the removed restraint and reaction force R in the most loaded adjacent restraint when DIF and DIF* are considered on every span and the spans above the removal only. A similar procedure was also proposed by Freddi *et al.* [36] for the axial force in central column removal. The following formulations were obtained for the displacement above the removal δ and the axial force in the column adjacent to the removal N:

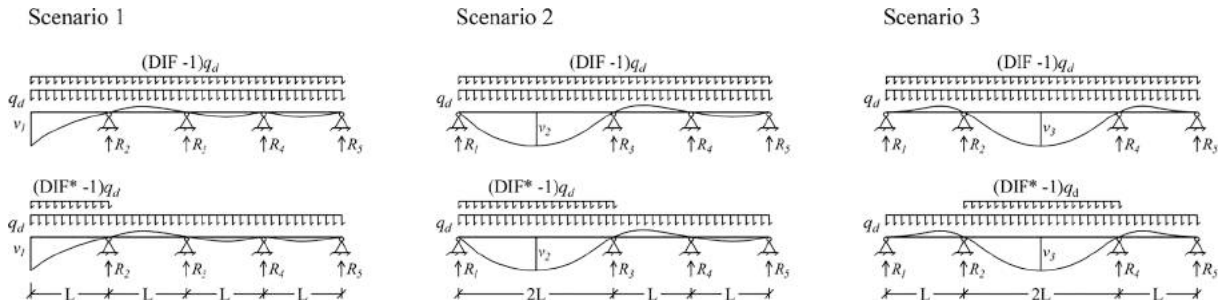

Fig. 5. Static schemes for the definition of DIF* from DIF.

$$\begin{aligned} &\text{Scenario 1} \quad \mathrm{DIF}^*_\delta = 88/97 \cdot \mathrm{DIF}_\delta + 9/97; \quad \mathrm{DIF}^*_N = 61/49 \cdot \mathrm{DIF}_N - 12/49 \\ &\text{Scenario 2} \quad \mathrm{DIF}^*_\delta = 64/67 \cdot \mathrm{DIF}_\delta + 3/67; \quad \mathrm{DIF}^*_N = 93/74 \cdot \mathrm{DIF}_N - 19/74 \\ &\text{Scenario 3} \quad \mathrm{DIF}^*_\delta = 13/16 \cdot \mathrm{DIF}_\delta + 3/16; \quad \mathrm{DIF}^*_N = 57/40 \cdot \mathrm{DIF}_N - 17/40 \end{aligned} \tag{5}$$

The DIF offers the advantage of being relatively easy to incorporate into the analysis process. Since it applies to the loads on each floor, it can be directly included in the load combination. By amplifying the load combination with the DIF a simple gravity analysis of the MRF becomes sufficient to account for dynamic effects. However, the application of incremented loads only to the region above the column loss through the DIF* prevents from inducing higher forces and displacement in regions that should be less affected by dynamic effects. Hence, the use of DIF* in static removal analysis is suggested.

4. Discussion of the results

The following section synthetically presents and discusses the results related to the assessment of dynamic effects. The results are critically examined, considering the different collapse mechanisms observed. The obtained dynamic increase factors are compared against the state-of-the-art and current recommendations.

4.1. Pushdown analyses and failure mechanisms

Fig. 6 shows the results of the pushdown analyses on the five case study MRFs considering Scenario 3 (*i.e.,* central column loss - see Fig. 1). The evolution of beam and column mechanisms are depicted in Fig. 6(a) and (b), in which the vertical displacement above the removal δ and the axial force in the most stressed column adjacent to removal N are shown. Analyses were run until collapse or incipient collapse, which was observed at different λ values, *i.e.,* 1.46, 1.35, 1.14, 1.07, and 1.06 for the 3 to 15-story MRFs.

The displacements and the axial forces are normalized with respect to the displacement and axial force capacities δ_m and N_b to highlight which parameters are critical to the stability of the structures. The displacement δ_m is attained at the maximum bending moment M_m (see Fig. 2(c)). The buckling resistance $N_{b,Rd}$ for the weak axis according to EN1993-1-1 [63] may be significantly different from the actual buckling resistance owing to the effect of combined weak and strong axis imperfections, the stiffness contribution of the structure surrounding the column, and the interaction with the shear and bending moments induced by the loading pattern. Therefore, the column buckling resistance N_b was evaluated with numerical analyses by applying single vertical forces on the top of the ground story columns on the fully damaged MRFs and measuring the vertical reaction at the ground story of the relevant column. These analyses allowed for accounting for the combined weak and strong axis imperfections and the stiffness contribution of the remainder of the structure. The results of these analyses are reported in Table 2.

Fig. 6(a) shows that in Scenario 3, the displacements δ for MRFs with >6 stories do not reach their capacities throughout the analysis and remain below 30 % of δ_m. Conversely, for the 3-story MRF, failure occurs, and the plastic hinge is fully developed. Fig. 6(b) shows that failure can be attributed to the buckling of the columns for MRFs with >6 stories since the axial force N attains the reference buckling resistance N_b. On the other end, for the 3-story MRF, the axial force remains below 70 % of N_b.

Fig. 7 synthetically shows the evolution of the different failure mechanisms for all case study structures and the three column loss scenarios. The left subplots of Fig. 7(a) to (c) show the development of the column buckling mechanism. The axial force of the most stressed column adjacent to the column removal is plotted against the out-of-plane displacement of the middle node of the column ($u_{y,col}$). At the same time, the instances related to $\lambda = 1$ are reported in the plots. In all scenarios, a linear force–displacement response is

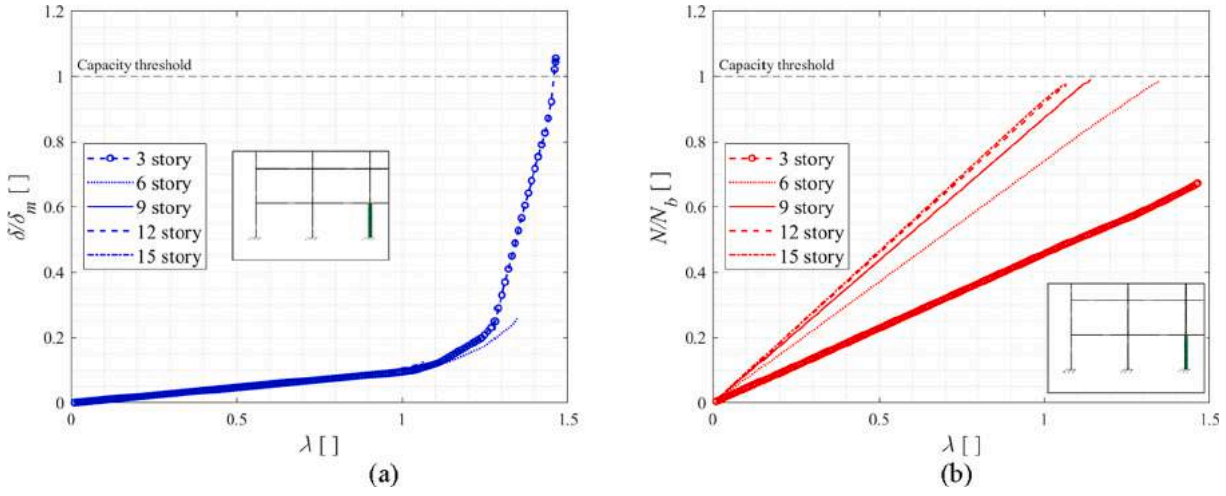

Fig. 6. Pushdown analyses. Central column loss scenario - Scenario 3: (a) vertical displacement of the beam above column removal; (b) axial force of the most stressed column.

Table 2
Ground story column buckling resistance.

N. of stories	Scenario	EN1993-1-1 [63] $N_{b,Rd}$ [kN]	Numerical simulation N_b [kN]
3	1		2632
	2	2686	2632
	3		2633
6	1		3277
	2	3357	3278
	3		3279
9	1		4076
	2	4245	4078
	3		4078
12	1		5033
	2	5104	5036
	3		5036
15	1		6000
	2	6074	6002
	3		6002

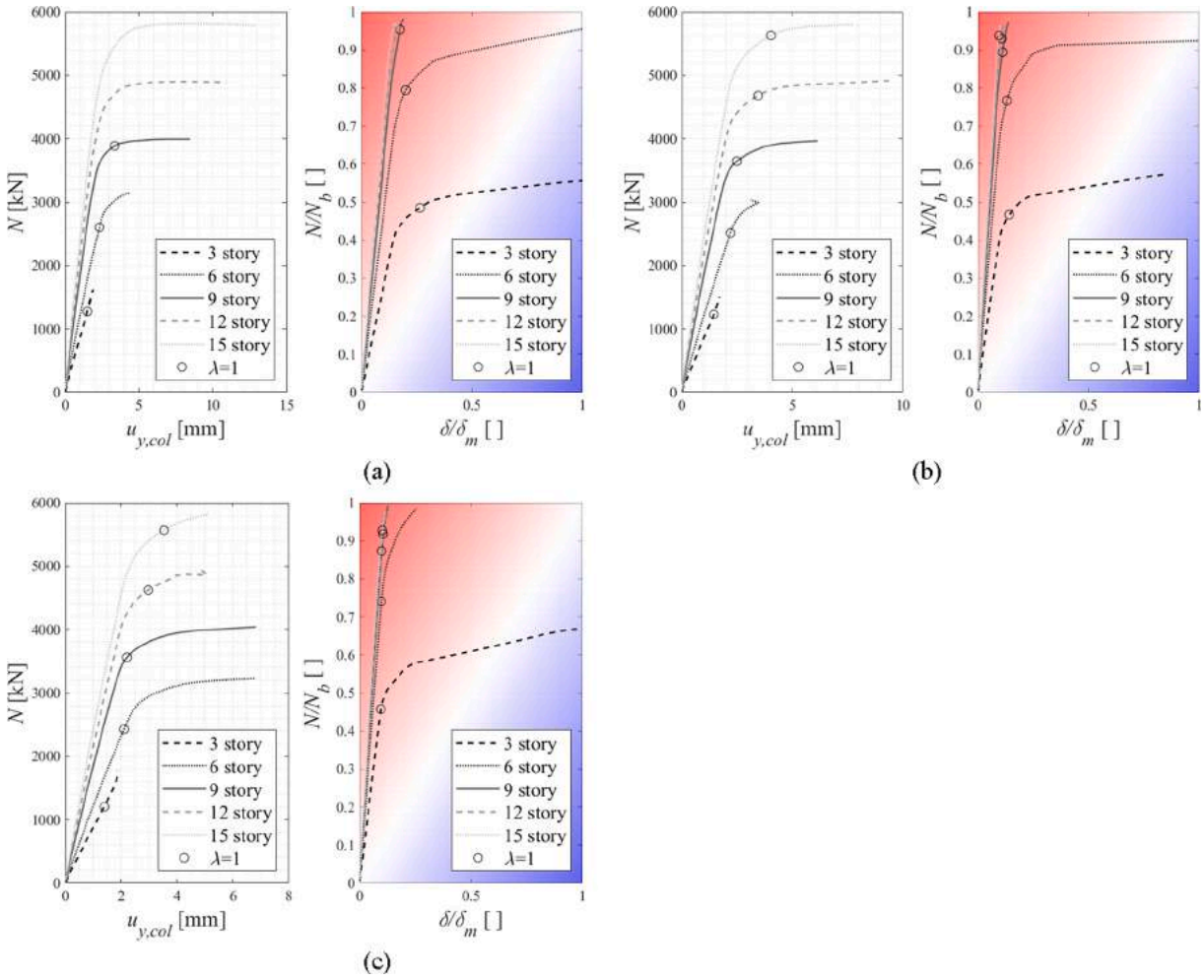

Fig. 7. Pushdown analyses. Buckling evolution and beam vs. column capacity plots: (a) Scenario 1; (b) Scenario 2; (c) Scenario 3.

observed for the 3-story MRF, *i.e.,* no buckling. Conversely, fully developed buckling appears for MRFs with >9 stories and is more marked in Scenario 1, in which runaway out-of-plane displacements occur for the 12- and 15-story MRFs. Large out-of-plane displacements caused by column buckling are only measured for the 6-story MRF in Scenario 3.

The right subplots of Fig. 7(a) to (c) synthetically represent the development of beam and column mechanisms. These plots compare the demand-capacity ratios for the column axial force N/N_b and the displacement above removal δ/δ_m, providing insights into the mutual evolution of the beam and column mechanisms throughout the analyses. The shaded regions indicate the primary governing mechanism at collapse, where red and blue are, respectively, for the column and beam mechanisms. The column mechanism develops when the columns exhibit loss of stability due to excessive lateral or out-of-plane displacements induced by the attainment of the buckling resistance. Conversely, the beam mechanism entails the development of plastic hinges at the beams ends followed by catenary action.

In all scenarios, for the 3-story MRF, the beam mechanism is predominant since displacements start to increase rapidly when column buckling is still not significant (*i.e.,* $N/N_b < 0.6$). Conversely, in MRFs with >9 stories, the column mechanism becomes more relevant since axial forces close to N_b are attained at failure. In these MRFs, the displacements increase, but the full sectional capacity is not exploited, and displacements remain well below δ_m. In the 6-story MRF, both column and beam mechanisms significantly contribute to the failure of the structure, while the failure is mainly related to column buckling in Scenario 3. As a final remark, it is noteworthy that in Scenario 1, the 12- and 15-story MRFs could not redistribute the loads defined according to Eq. (1) since failure was attained before the complete application of the load, *i.e.,* $\lambda < 1$. The primary mechanism involved in the collapsing phase and the load factor at failure are summarized in Table 3.

4.2. Non-linear dynamic analyses

Fig. 8 and Fig. 9 show the results of the dynamic analyses for the two identified EDPs. Analyses were performed for the three scenarios for increasing values of the coefficient λ with constant increments equal to 0.1. For the sake of brevity, only the results for 3-, 9-, and 15-story MRFs, representative of low-, medium-, and high-rise buildings, are shown extensively. For graphical purposes, it was assumed that the static 'state restoring' analysis, *i.e.,* Step 2 of the dynamic procedure, is performed in 1 s, after which the dynamic removal force is applied.

Fig. 8 shows that the magnitude of the vertical displacement δ increases with the load factor λ and decreases with the number of stories of the MRFs. The results depicted with dashed lines represent those obtained after buckling is observed in the column adjacent to the removal. When buckling occurred, but the full target load factor could not be applied, the analysis was terminated, and the last result is indicated with a red cross. In this situation, no meaningful peak response could be measured, and the analyses were discarded. In other cases, after the onset of buckling, the column is gradually unloaded, and loads are redistributed to the other columns until collapse occurs while ever-increasing displacements δ are measured. These analyses could not be considered to evaluate the dynamic effects on the displacements.

Since higher loads were associated with higher masses, the load factor λ also affects the vibration period in the dynamic analyses. The peak response is indicated with black points and typically occurs after the same number of oscillations regardless of the load factor. In Scenario 1, the perimetral column removal induces a lateral oscillation of the structures that may affect the vertical displacement above the removal. This effect becomes particularly relevant for higher MRFs, causing the peak dynamic response to appear at oscillations >1. Moreover, in a few cases, plasticity also propagates after these oscillations, and the displacement δ increases until energy dissipation prevents obtaining higher displacements. Larger peak displacements were observed in low-rise MRFs, in which the development of the beam mechanism was more marked.

Fig. 9 shows that the magnitude of axial forces N increases with the number of stories of the MRFs. For high λ values, buckling was observed in the columns for forces approaching the reference column buckling resistance N_b. Typically, in each MRF the peak forces are obtained after the same number of oscillations. Hence, for cases that do not experience buckling, the time at which the peak response is measured increases with the load factor, as the period increases when λ increases. For cases experiencing buckling, for higher load factors, the maximum load is reached at an earlier step as column buckling resistance N_b cannot be exceeded.

Table 3
Pushdown analysis. Failure mechanisms.

N. of stories	Scenario	Failure mechanism	λ at failure
3	1	Beam	1.37
	2	Beam	1.24
	3	Beam	1.46
6	1	Beam & Column	1.21
	2	Beam & Column	1.21
	3	Column	1.35
9	1	Column	1.04
	2	Column	1.09
	3	Column	1.14
12	1	Column	**0.96**
	2	Column	1.06
	3	Column	1.07
15	1	Column	**0.92**
	2	Column	1.04
	3	Column	1.06

Note: In bold cases where failures occurred before full load application.

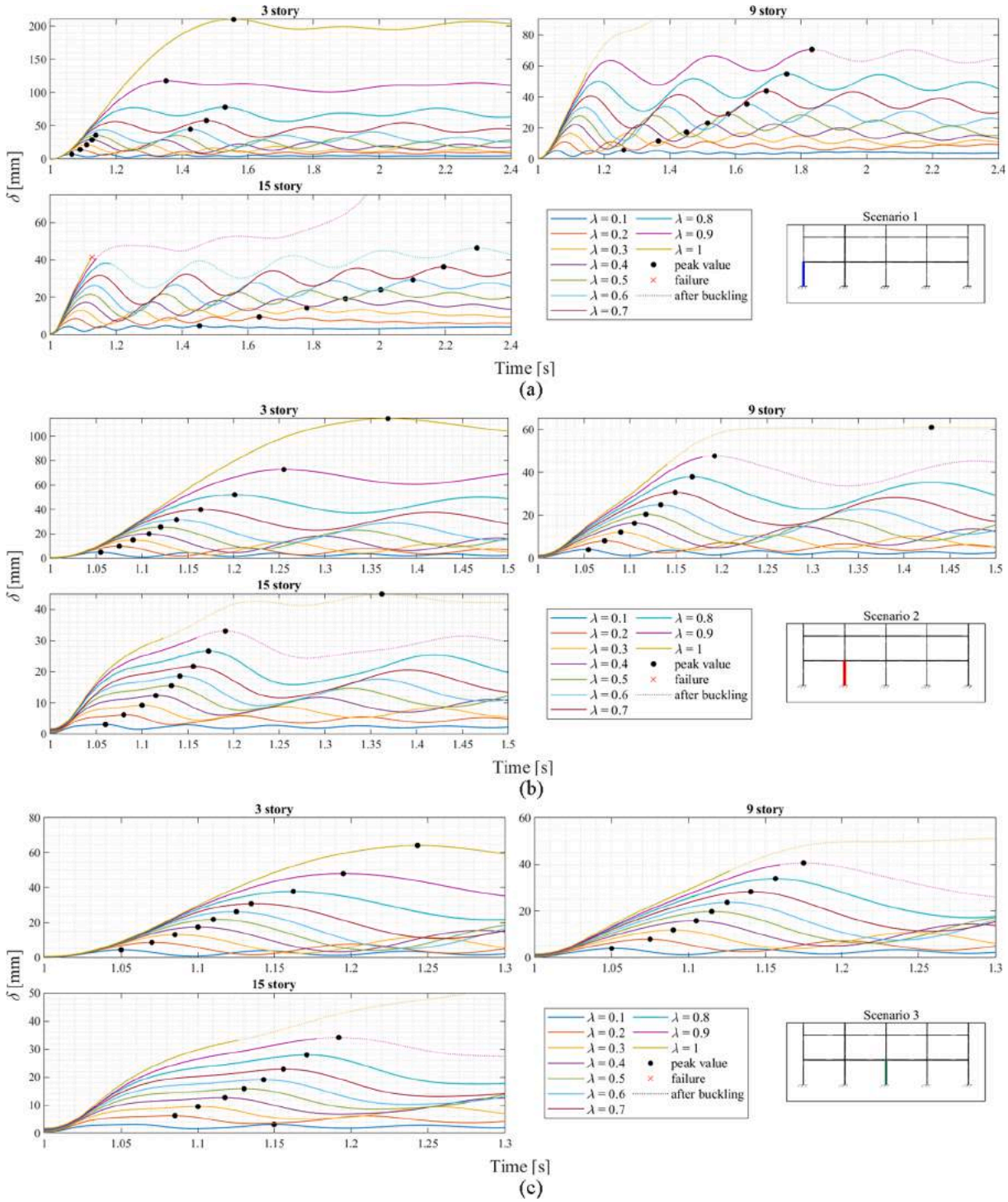

Fig. 8. Non-linear dynamic analyses. Vertical displacement of the node above removal for the 3-, 6-, and 9-story structures: (a) Scenario 1; (b) Scenario 2; (c) Scenario 3.

For the 3-story MRF small additional oscillations can be observed in the first part of the axial force response. This is related to the inelastic behavior of beams and becomes particularly evident for high λ values. Such response is peculiar of structures prone to the beam mechanism and was observed also for the 6-story MRF, especially in Scenario 1 and 2, when the development of plastic hinges was involved in the collapse behavior.

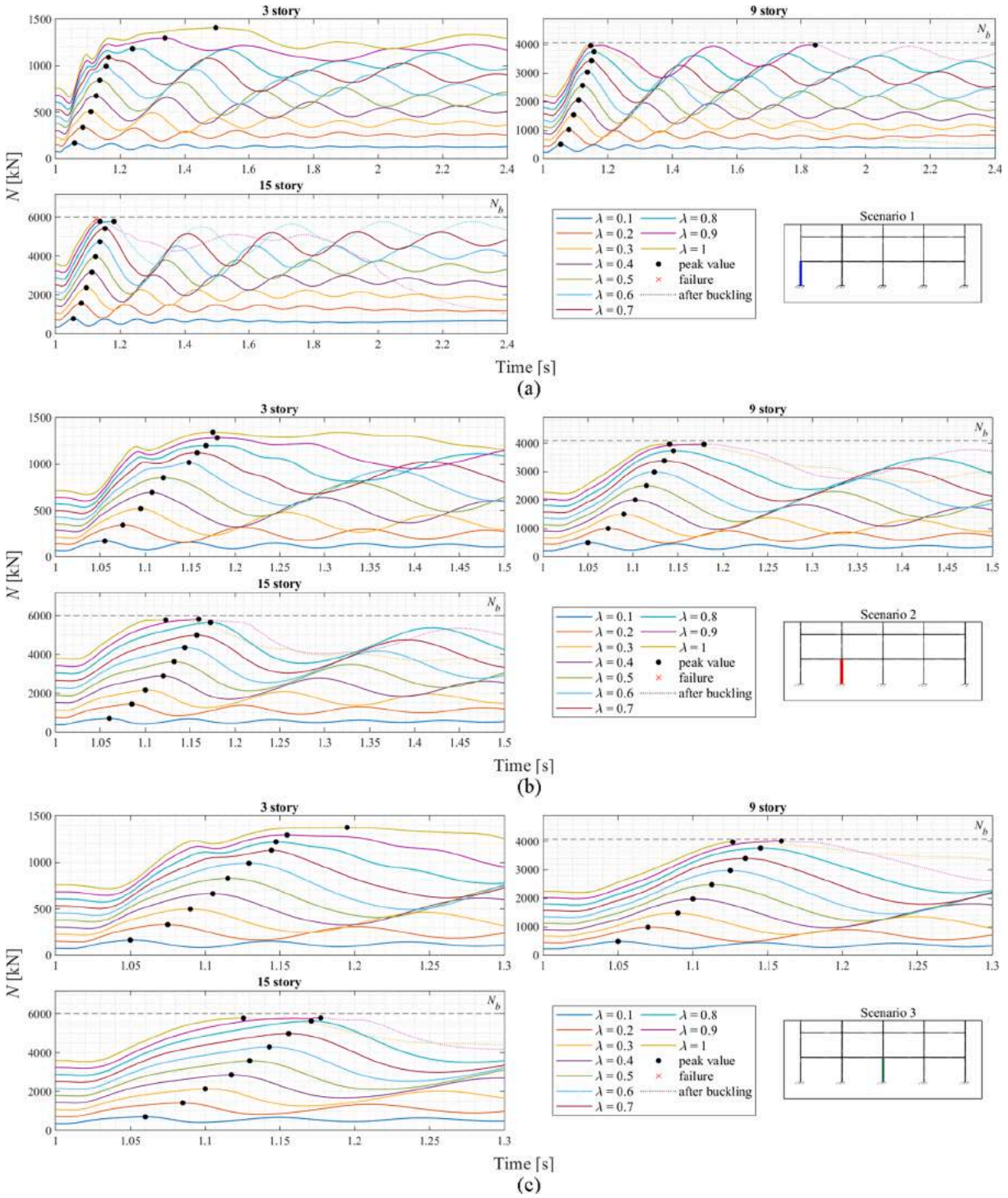

Fig. 9. Non-linear dynamic analyses. Axial force in the column adjacent to the removal for the 3-, 6-, and 9-story structures: (a) Scenario 1; (b) Scenario 2; (c) Scenario 3.

4.3. Peak dynamic vs. static response

The influence of the dynamic effects has been assessed by comparing the peak EDP values obtained for the static and dynamic procedures across the whole range of load factors investigated. For the sake of brevity, the comparison is provided only for the 3-, 9-, and 15-story MRFs.

Fig. 10 shows the comparison in terms of peak dynamic displacements (blue continuous line) and static displacements (blue dashed line). The analyses in which column buckling was observed, but the structure did not eventually collapse, are indicated in grey. Circles show the situation in which the same target displacement value $\overline{\delta}$ was obtained in the dynamic and static analyses. For the dynamic analyses these values are the displacements obtained at the target load factors $\overline{\lambda}_i$ employed in the IDA analyses, *i.e.*, $\overline{\delta}_i = \delta_{D,i} = \delta_D(\overline{\lambda}_i)$

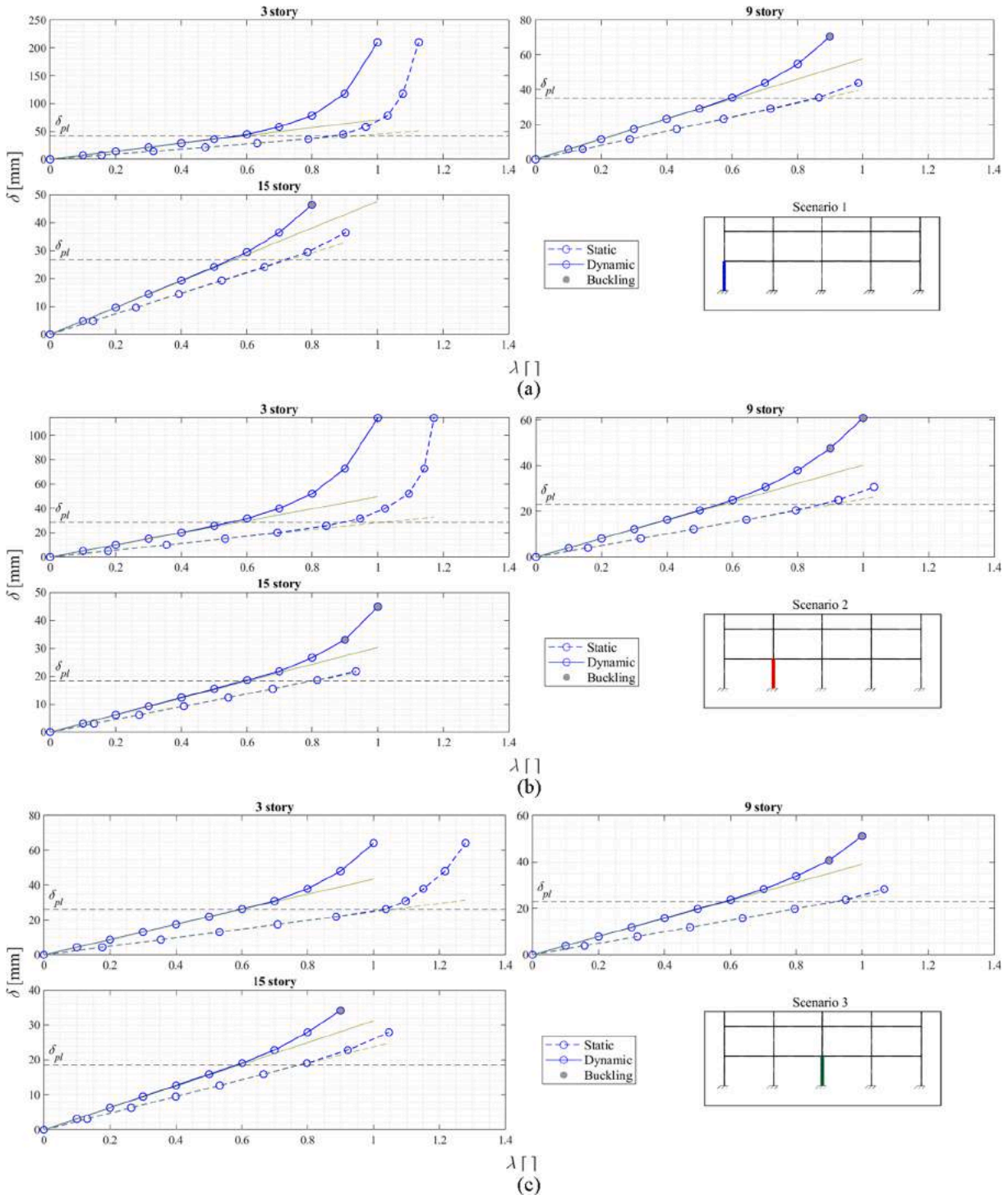

Fig. 10. Static vs. Dynamic analyses. Vertical displacement of the node above removal for the 3-, 6-, and 9-story structures: (a) Scenario 1; (b) Scenario 2; (c) Scenario 3.

with $\bar{\lambda}_i = 0.1–1$. It can be observed that the static response δ_S equals the peak dynamic response δ_D for higher values of the load factor λ. In general, the peak dynamic response is always higher than the static one owing to the dynamic effects induced by the sudden application of the removal force. For the sake of simplicity, static results exceeding the highest peak dynamic value δ_D are not shown as they cannot be used in Eq. (4).

The green lines represent the initial linear trend, while the results show a non-linear evolution for higher load factors. In the non-

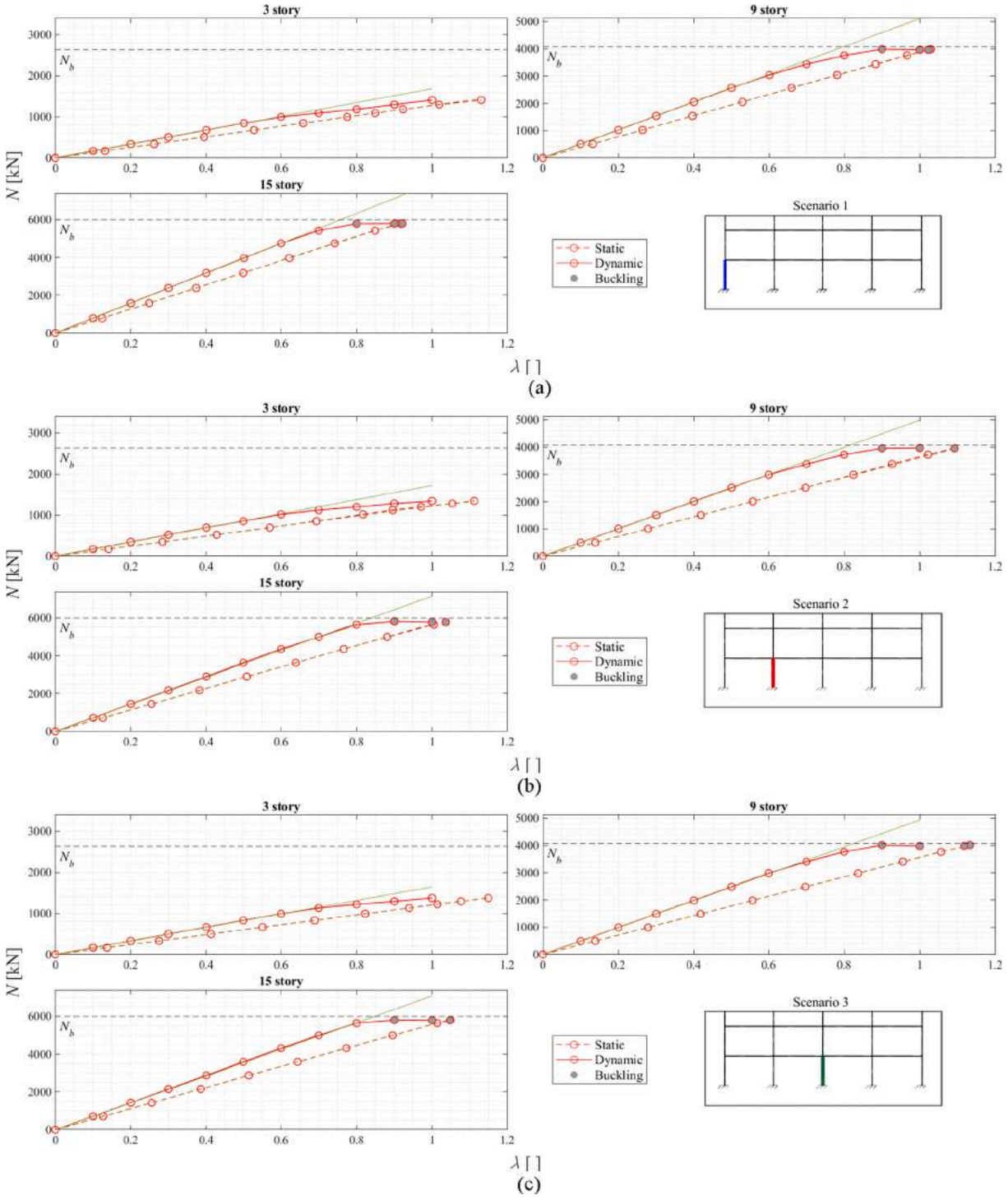

Fig. 11. Static vs. Dynamic analyses. Axial force in the column adjacent to the removal for the 3-, 6-, and 9-story structures: (a) Scenario 1; (b) Scenario 2; (c) Scenario 3.

linear range, the displacement tends to increase more rapidly owing to the exceedance of the plastic moment in the beams above the column removal at δ_{pl}. Hence, since the non-linear evolution of displacements is related to the spread of plasticity and owing to the response amplification induced by dynamic effects, the non-linear behavior initiates for lower values of λ in the dynamic analyses. Moreover, only the 3-story structure exhibits a marked non-linear evolution of the displacement, induced by the full development of plastic hinges.

Fig. 11 shows the comparison in terms of peak axial forces. The analyses in which column buckling occurred are indicated in grey. In this case, also the analyses in which the structure eventually collapsed are considered since the peak response can be used to derive the dynamic increase factors. As observed for the peak displacements in Fig. 10, the peak dynamic response is always higher than the static one also for the axal force, due to the higher response generated by the inertial effects. In contrast with the continuously growing displacements, this figure shows a slow increase of the axial forces as they approach the actual buckling capacity. The results indicated with circles show that the static response N_S equals the peak dynamic response N_D for higher values of the load factor λ. Collapse occurs for axial forces approaching the buckling resistance N_b, except for the 3-story MRF. In this frame, the beam mechanism is predominant and causes collapse for dynamic forces N_D and static forces N_S well below N_b.

The axial force shows a non-linear evolution when approaching the buckling resistance N_b. However, it is interesting that the 3-story structure shows a non-linear evolution of the peak dynamic axial force even if columns are less stressed. In this frame, the beam mechanism leads to significant beam rotations (see Fig. 7), favoring a high concentration of energy dissipation at the beam ends. This contributes to damping the dynamic response, and therefore, the dynamic forces transmitted to the columns are reduced, gradually approaching the magnitudes observed in static analyses. This is confirmed by the fact that in the 3-story MRF, the non-linear evolutions of the dynamic axial force in Fig. 11 and displacement in Fig. 10 start at the same load factor λ. In the 9- and 15-story buildings, energy dissipation in plastic hinges is less relevant.

4.4. Dynamic increase factors (DIF and DIF*)

DIF values were calculated with the load-based approach shown in Eq. (4) for all case study structures and all scenarios. The associated DIF* were derived from the linear transformations specified in Eq. (5). Fig. 12 depicts the procedure for the derivation of DIF, considering only the displacement for simplicity. For a selected load factor $\bar{\lambda}_i$ the associated peak dynamic displacement $\delta_D(\bar{\lambda}_i) = \bar{\delta}_i$, indicated with the horizontal line, is taken as target displacement. The load factor necessary to reach the target displacement in the static analysis $\lambda_S(\bar{\delta}_i)$ is employed together with $\lambda_D = \bar{\lambda}_i$ in Eq. (4) to derive DIF($\bar{\lambda}_i$). The response values relevant to the calculation of the DIF are shown with black points. To obtain the same displacements in the static and dynamic analyses the DIF($\bar{\lambda}_i$) should be introduced in the static analysis when the load factor to be applied is $\bar{\lambda}_i$, or when the static demand on the structure with no load amplification reaches $\delta_S(\bar{\lambda}_i)$, as shown with the red cross.

The dynamic increase factors can be determined from the target load factor before any analysis is performed, *i.e.*, *a priori* definition, while a static analysis is necessary to determine the static demand with unamplified loads (*e.g.*, $\delta_S(\bar{\lambda}_i)$) and derive the associated dynamic increase factor, *i.e.*, *a posteriori* definition. However, the load factor depends on how loads are defined (live loads, dead loads, etc.) and combined, and therefore, associating dynamic increase factors to the load factor does not allow for generalization. Conversely, the static demand is a measure that is independent from the loads and describes the exploitation of the characteristics of the specific structure (*i.e.* demand/capacity ratios). Moreover, considering demand/capacity ratios it is easier to track the evolution of the dynamic increase factors in respect to the development of the relevant mechanisms.

For these reasons, in Fig. 13 it was preferred to represent DIF and DIF* in respect with the demand/capacity ratios of the relevant structural elements (beams and columns). Fig. 13 shows for every scenario, the DIF and DIF* obtained for each of the EDP target value

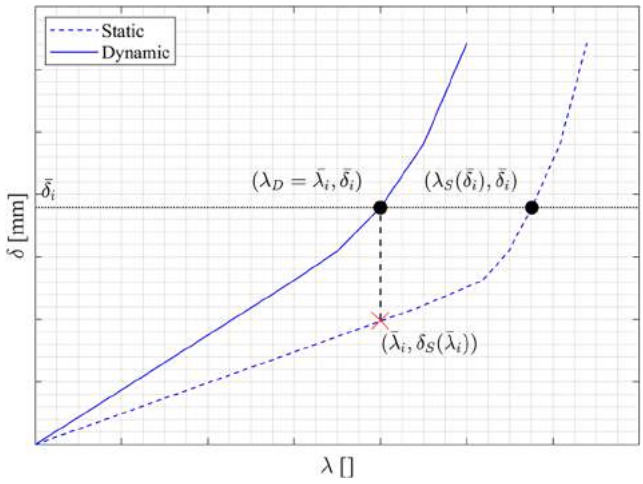

Fig. 12. Dynamic increase factor derivation procedure.

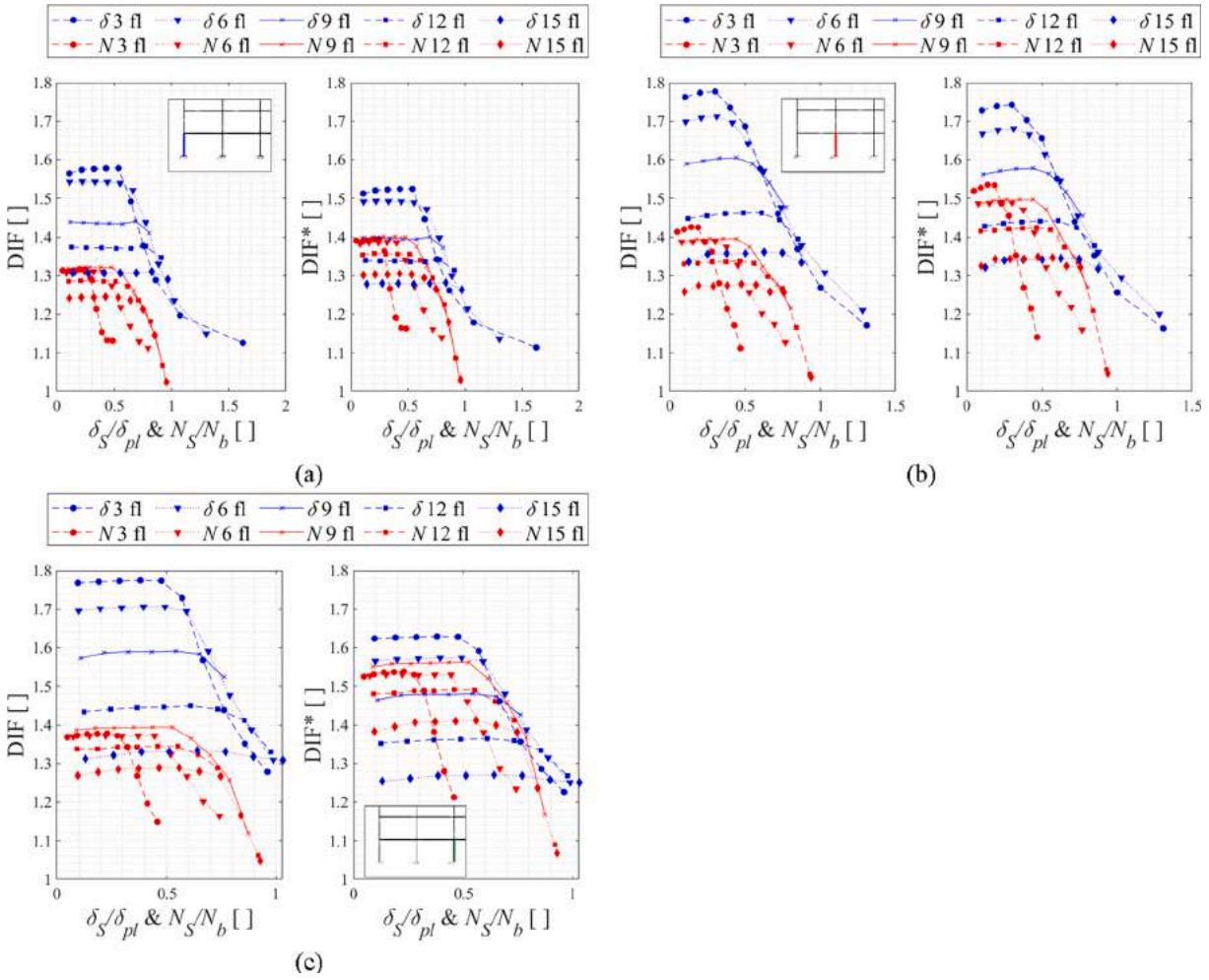

Fig. 13. DIFs and DIF*s vs structural demand in pushdown analyses: (a) Scenario 1; (b) Scenario 2; (c) Scenario 3.

$\overline{\delta}_i = \delta_{D,i} = \delta_D(\overline{\lambda}_i)$ and $\overline{N}_i = N_{D,i} = N_D(\overline{\lambda}_i)$, indicated with circles in Fig. 10 and Fig. 11. These dynamic increase factors apply to structures in which the EDP values measured in the static analyses are $\delta_S(\overline{\lambda}_i)$ or $N_S(\overline{\lambda}_i)$. Hence, Fig. 13 shows the evolution of DIF and DIF* with the static structural demand $\delta_S(\overline{\lambda}_i)/\delta_{pl}$ and $N_S(\overline{\lambda}_i)/N_b$. The demand is quantified with respect to δ_{pl} and N_b, since as shown in Fig. 10 and Fig. 11 non-linear behaviour appeared when the response was close to these quantities. It should be observed that for the specific loads considered in this study it is still possible to identify the dynamic increase factors from the load factors $\overline{\lambda}_i$ in Fig. 13. Indeed, markers show the DIF values calculated at each load factor $\overline{\lambda}_i = 0.1$–1.

The typical behavior of the dynamic increase factors involves an initial almost constant branch followed by a non-linear branch with decreasing values. The dynamic increase factors remain essentially constant until both the peak dynamic and static response show a linear trend in Fig. 10 and Fig. 11. Once the non-linearities appear in the dynamic response, the dynamic increase factors start to decrease until minimum values are reached at collapse. In the initial branch the perimetral column removal scenario (Scenario 1) exhibits lower dynamic increase factors, while similar values are observed for the other scenarios.

The values of the initial branch decrease with the number of stories when the displacement δ is considered. Conversely, when the axial force N is considered, this trend remains valid only for frames whose collapse is governed by column buckling (9–15 stories). Moreover, for 3- and 6-story structures, the dynamic effects are reduced for lower values of N_s/N_b, when large rotations appear in the beam ends. The high concentration of energy dissipation in these regions induces an additional damping effect, reducing the dynamic forces transmitted to the columns.

Except for the different initial branches, whose values are influenced by the effects of damping and the characteristics of the frame, in buckling-governed MRFs (9- to 15-stories) the dynamic increase factors for the axial force converge to the same values in the non-linear branch. Conversely, for the 3- and 6-story frames, the significant reduction in the dynamic increase factors for the axial force is still governed by the development of the beam mechanisms. In all structures, the factors derived for the displacement show a similar non-linear branch governed only by the onset of plastic hinges in the beams.

Dynamic increase factors for the axial force N span in a narrower range. It is interesting to note that the DIF is increased for N and

decreased for δ when the DIF* is derived. Indeed, loads on farther beams have a beneficial lifting effect on the vertical displacement δ. When loads are amplified only in the beams above removal, this lifting effect is reduced, and therefore, lower factors are required to achieve the same vertical displacement δ. On the other hand, a uniform amplification of the loads across all spans ensures that the same axial force obtained by increasing only the loads on the beams above removal is attained for lower increase factors. However, considering all scenarios, the range in which dynamic factors span is only slightly reduced, varying from 1.02 to 1.78 for the DIF to 1.03–1.74 for the DIF*.

4.5. Comparison with the state-of-the-art dynamic increase factors

The derived dynamic increase factors are compared with formulations provided in previous research. As research in literature mainly focused on dynamic increase factors considering only the response in terms of displacements, results in terms of axial forces could not be compared to existing studies. Conversely, previous studies showed that the dynamic increase factor is affected by the energy dissipation obtained in the structural components as a consequence of the plastic deformations. For this reason, the factors provided in existing analytical equations are often related to the ratio δ/δ_{pl} or $M_S/M_{pl.}$ In this context, comparison with two relevant formulation is presented in the followings. Finally, DIF* derived for both displacements and forces are compared to the factors recommended in the UFC guidelines [7].

4.5.1. Dynamic increase factors according to Tsai (2010)

In Fig. 14(a) the DIF values are compared with the formulation proposed by Tsai [58]. This formulation was derived with a force-based approach considering a bilinear elastic–plastic SDoF model with a post-elastic stiffness ratio α. In the showed curves only the ratio α (see Fig. 2) for the beams above removal of the 15-story frame was considered, since slightly lower values were associated to the beams of the other structures with little influence on the DIF curves. The proposed formulation is provided with respect to the displacement in the dynamic analyses, *i.e.,* the target displacement $\overline{\delta} = \delta_D$. The numerical results and formulation by Tsai are in good agreement, especially for Scenario 2 and 3. In general, numerical values are lower than the curve proposed by Tsai, owing in particular to the fact that damping was considered in the numerical simulation, emphasizing its beneficial effect in reducing the DIF.

Indeed, previous studies in literature highlighted the influence of damping in the evaluations of dynamic increase factors. The maximum reference value is 2 for a SDoF linear elastic undamped system, but it becomes lower when damping is considered [51]. Similarly, in Fig. 14(a) the maximum DIF values are obtained when the beams are still in the elastic range, *i.e.,* $\delta < \delta_{pl}$. In general, part of the vibrational energy is dissipated through various damping mechanisms, which can further reduce the dynamic responses, resulting in lower values of the dynamic increase factors. Inelastic buckling phenomena and the joints may have an influence on the dynamic response as well, as they might dissipate energy and induce a damping effect. These aspects contribute to the attainment of different DIF values depending on the building and the scenario.

4.5.2. Dynamic increase factors according to Liu (2013)

Fig. 14(b) presents a comparison between the DIF* values derived for the displacement δ with Eq. (5) and the formulation suggested by Liu [55]. This formulation was based on numerical simulations of three steel frames under an internal and a perimetral column removal. 9-story frames with five bays and no initial imperfections were considered. DIF* were compared with this formulation since numerical analyses performed by Liu implied the increment of the loads only of the bays above the removed column. The evolution of DIF* was expressed with respect to the ratio between the bending moment in the static analyses M_S and the plastic moment M_{pl}.

For Scenario 2 and 3 the numerical results are in good agreement with the proposal of Liu for the inelastic range in the dynamic

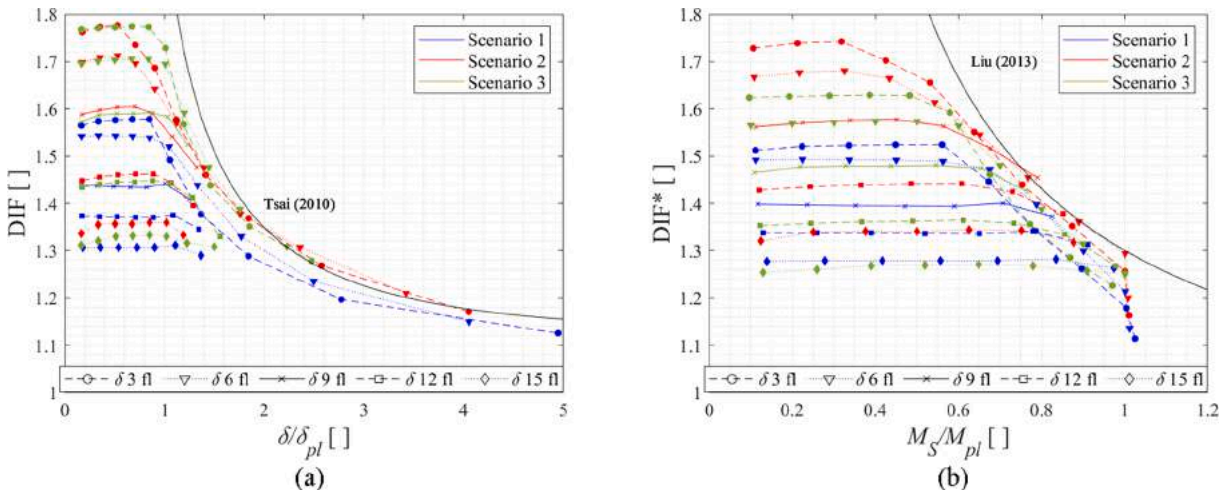

Fig. 14. Comparison of dynamic increase factors for δ against the state of the art: (a) DIF vs. Tsai (2010); (b) DIF* vs. Liu (2013).

analyses, *i.e.,* $M_S/M_{pl} > 0.5$. Indeed, it was found that the lowering of the beam ends induced by column buckling did not significantly affect the displacements δ, and therefore, results for the DIF* are comparable to those presented in [55] even if imperfections were not introduced in this work. The value for entering the inelastic range was set considering the conventional DIF* of 2 for the elastic range and that at the elastic limit ($M_D = M_{pl}$) the simplification $M_D(\lambda) = M_S(\text{DIF}^*\cdot\lambda) = \text{DIF}^*\cdot M_S(\lambda)$ can be accepted.

Few results were available in the static post-elastic range in Liu's analyses and no specific formulation was provided for $M_s/M_{pl} > 1$. However, in a recent work [57] a significant reduction of the DIF* with an analogous behavior to the one exhibited by low-rise MRFs in Fig. 14(b) was found in this range. This change in the behavior is mainly devoted to the static analyses entering the inelastic range for $M_s/M_{pl} > 1$, adding a further source of non-linearity in the evolution of DIF*.

For Scenario 1 the derived DIF* values are significantly lower than Liu's formulation. Similarly, Liu found that the lowest numerical DIF* in his analyses were obtained with a perimetral column removal, in particular for $M_S/M_{pl} \leq 0.5$. According to Liu [55], this fact can be attributed to the higher level of geometrical non-linearity introduced by the removal of an exterior column and the subsequent redistribution of gravity loads among a smaller number of bays, which may contribute in reducing the dynamic response.

It should be observed that for $M_S/M_{pl} \leq 0.5$ the numerical results show different levels of dynamic increase factors depending on the structures. This highlights that already in the elastic range, the dynamic response varies with the level of geometric non-linearity of the structure and that damping effects might reduce the response more significantly for low-rise structures. Liu [55] proposed different linear branches which were however obtained only from the analyses of one seismically designed MRF with 9-story and are therefore not reported in Fig. 14(b).

4.5.3. *Dynamic increase factors according to UFC*

In Fig. 15 factors associated with the same state, *i.e.,* same load factor, are compared more concisely for two selected load factors, *i.e.,* $\lambda = 0.4$ and $\lambda = 0.7$ respectively. Among all the investigated cases, $\lambda = 0.4$ was identified as the highest load factor for which the variation of the dynamic increase factors is not significant, while $\lambda = 0.7$ is the highest load factor for which buckling did not occur.

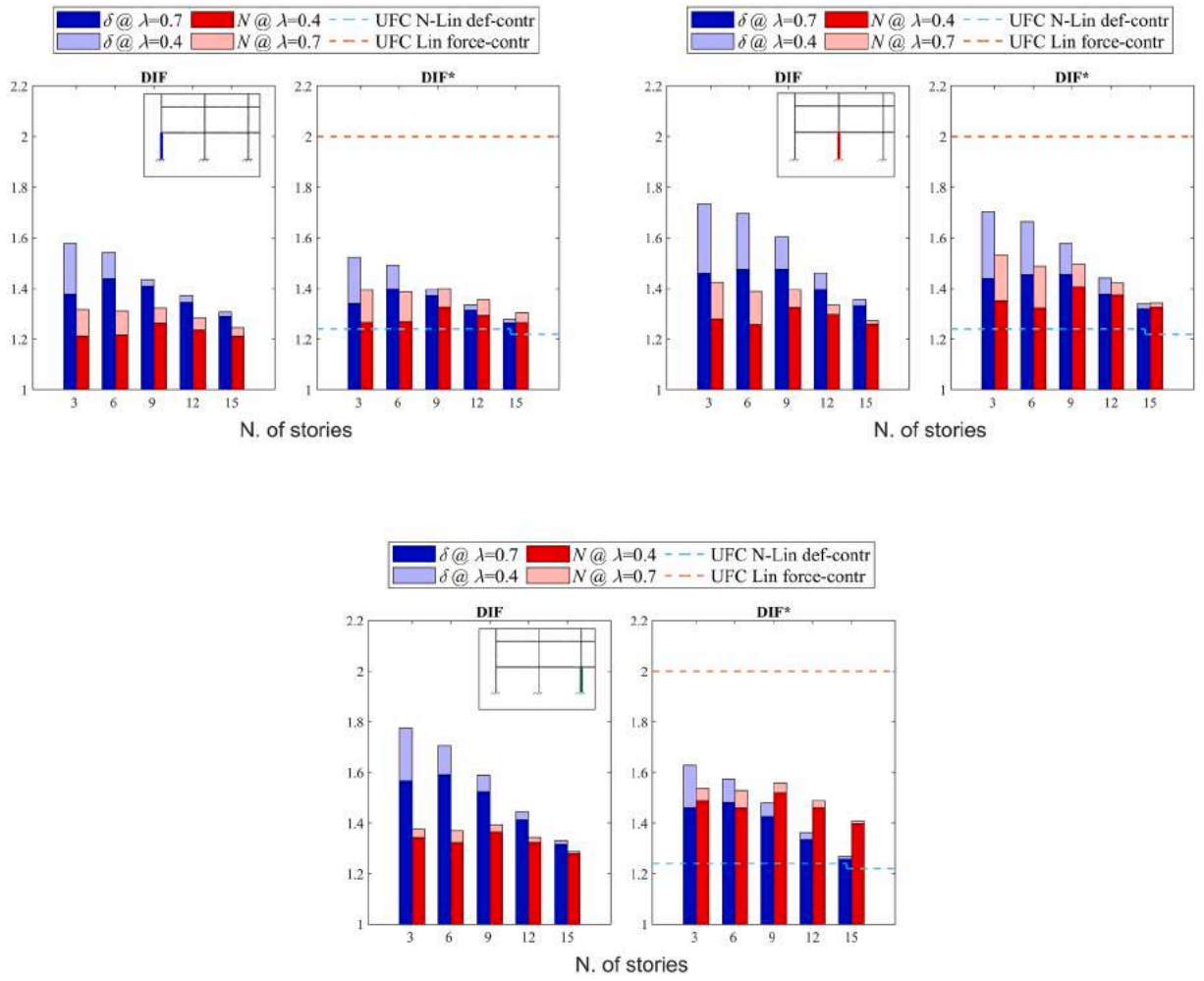

Fig. 15. Dynamic Increase Factors at $\lambda = 0.4$ and $\lambda = 0.7$: (a) Scenario 1; (b) Scenario 2; (c) Scenario 3.

In the case of $\lambda = 0.4$, DIF is always higher for the displacement. However, when only loads above the removal are amplified through the DIF*, the highest value among the one for the displacement and the axial force is better aligned with the critical mechanism. When the beam mechanism is more relevant (3- and 6-story buildings), the DIF* for the displacement is typically higher than the one for the axial force, and *vice versa* when the column mechanism is critical (9-, 12-, and 15-story buildings). There are few exceptions, *i.e.,* the 9- and 12-story MRFs in Scenario 2, and therefore a direct correlation between the collapse mechanism identified in the pushdown analyses (shown in Fig. 7) and the DIF* cannot be established.

In Fig. 15 the derived dynamic increase factors are compared with the ones recommended in the UFC guidelines [7]. These guidelines provide dynamic increase factors to be applied on the region above the removal and are therefore compared with DIF*. Moreover, it should be mentioned that a force-based approach was employed in the derivation of the UFC factors and therefore, the comparison with the factors presented in this study is consistent.

The UFC [7] provides a formulation for the dynamic increase factors to check deformation-controlled actions in non-linear static analyses which depends on the material and mechanical properties of the affected structural members and its ductile behavior. This formulation considers the ratio between the plastic rotation angle θ_{pra} defined in acceptance criteria provided in [7] and yield rotation θ_y in any primary element, component, or connection in the model within the area that is loaded with the increased gravity load. The highest among the obtained factors should be considered, which for the case study structure was 1.24, except for the 15-story structure, for which 1.22 was obtained. These values were determined considering that the structures have welded unreinforced flanges connections.

No separate calculation is provided in the UFC [7] to account for brittle failures as column buckling in non-linear static analyses, and the same value is suggested for both deformation- and force-controlled actions. On the contrary, for linear static analyses, a single value of 2 is suggested for force-controlled actions. In the absence of specific indications regarding non-linear analyses, the value of 2 can be conservatively taken for force-based mechanisms or brittle failures.

It is noteworthy that for $\lambda = 0.4$ the UFC values for deformation-controlled actions in non-linear analyses considerably underestimate the dynamic effects for the displacements. The dynamic effects are reduced at $\lambda = 0.7$ but are still higher than the UFC reference values. Hence, UFC deformation-controlled value underestimates the dynamic effects in particular when beams still not entered the inelastic range, but become more precise for load levels that significantly engage the structures.

On the other hand, as expected the UFC factor for force-controlled actions in linear analyses, *i.e.*, 2, significantly overestimates the DIF* for the axial force as it is based on the dynamic response of a SDOF at-rest linear elastic system [51]. A better estimate though conservative, can be obtained by considering the UFC values for displacement-controlled actions in non-linear analyses. The UFC factors are in better agreement with the numerical DIF^*_N for higher load factors, in particular when the beam mechanisms is more relevant, *i.e.,* for the 3- and 6-story buildings. It may be concluded that by applying UFC [7] factors, neither the displacements nor the axial force induced by dynamic effects can be accurately considered.

Finally, it should be observed that it is very difficult to propose a single value of the increase factor valid for all the situations. The impact of dynamic effects depends on the number of stories and the activated mechanisms, the column loss scenario, and the load factor. In general, the derived DIF* are meaningful for both δ and N and the most appropriate one should be determined based on the actual collapse mode or dominant mechanism of the investigated structure. As an alternative, the dynamic increase factor may be selected among factors derived for various EDPs, depending on the desired effect to maximize or deemed more significant in a specific case.

5. Conclusions

This paper investigates the dynamic effects in progressive collapse scenarios by evaluating the Dynamic Increase Factors for different steel structures with an increasing number of stories. A numerical procedure involving non-linear static and dynamic analyses was proposed and applied to evaluate the factors for five seismically designed case study Moment Resisting Frames (MRFs). Detailed finite element models were developed in OpenSees including mechanical and geometrical non-linearities. The models have been validated to simulate with good confidence the axial force-bending moments interaction in the beams (*e.g.,* PPH - due to the catenary effects) and the column buckling. Such models have been used to simulate three different column loss scenarios. Considerations related to the dynamic effects were provided considering two key Engineering Demand Parameters (EDPs) aiming at evaluating the effects under beam-type collapse mechanisms and column buckling failure, respectively. Dynamic Increase Factors were assessed, also considering their application on all loads acting on beams (DIF) or only on those above the column removal zone (DIF*), as for the UFC [7] recommendations. The outcomes of the analyses provided insights into the involved phenomena, revealing that the Dynamic Increase Factors might significantly differ from those recommended by the UFC guidelines [7]. In detail, relevant considerations are:

- The factors derived are meaningful for both δ and N and the most appropriate one may be determined based on the actual collapse mode of the investigated structure or the effect deemed more relevant in a specific application. Conversely, the indiscriminate application of the highest available DIF* may lead to a premature collapse of the structure. Hence, as also suggested in UFC [7] for deformation and force-controlled actions, it is recommended that both beam and column mechanisms are checked separately.
- The UFC [7] recommendations are unable to adequately account for the diverse dynamic responses exhibited by structures with different characteristic and structural demand, especially those prone to column buckling. The values suggested for non-linear analyses, which primarily address collapse considerations associated with beam mechanisms, tend to underestimate the dynamic effects measured on both the displacement δ and the axial force N. On the other hand, the single conservative value provided for linear force-controlled mechanisms largely overestimates the DIF* for the axial force.

- In the linear elastic range, the highest among the DIF* for the displacement and the axial force is generally the one related to the most critical mechanisms involved. Conversely, since the DIF values for the displacements δ were always higher than the ones for the axial force N, the DIF could not provide information about the mechanism governing the structural behavior.
- In structures in which the beam mechanism is predominant a high energy dissipation concentrates at the beam ends. This promotes a damping effect reducing the dynamic axial forces transmitted to the columns. Consequently, the magnitude of dynamic forces is gradually reduced when plastic hinges activate, causing a reduction of dynamic increase factors for the axial force N that is not related to the development of column buckling.
- The results showed that, as expected, for both the displacement and the axial force, the peak dynamic response is always higher compared with the static one, due to the inertial effects contribution. In the peak dynamic response, the non-linear behaviour appears for lower load factors, and eventually approaches the static one. This is evident when buckling is reached in the ground story columns, with the axial force approaching the buckling axial force N_b without exceeding it in both dynamic and static analyses. It was observed that the non-linear response is mainly initiated by the exceedance of the plastic moment M_{pl} in the beams above the column removal.

Finally, it was shown that the impact of dynamic effects depends on the number of stories and the main collapsing mechanism, and the column loss scenario. Damping may significantly affect the increase factors in the elastic range, with an increasing influence for an increasing number of stories. In the inelastic range, increase factors tend to a common path, but significantly lower values are obtained for perimetral column removals. Therefore, the definition of a general formulation for the DIF and DIF* is not straightforward. To offer detailed guidelines on dynamic effects, future work will include additional investigations supported by experimental studies. Moreover, to generalize the results various aspects will be considered in future studies, as the influence of different span lengths and interstorey heights and of the seismic design extending the analysis to non-seismically designed steel frames. Indeed, these frames are typically designed with more slender columns, which are therefore more sensitive to buckling. In addition, a further aspect that deserves a specific investigation is how the removal time and the damping ratio might impact the dynamic response and the Dynamic Increase factors.

CRediT authorship contribution statement

Luca Possidente: Writing – original draft, Visualization, Software, Methodology, Investigation, Formal analysis, Conceptualization. **Fabio Freddi:** Writing – review & editing, Supervision, Project administration, Methodology, Conceptualization. **Nicola Tondini:** Writing – review & editing, Supervision, Conceptualization.

Declaration of competing interest

The authors declare the following financial interests/personal relationships which may be considered as potential competing interests: Luca Possidente and Fabio Freddi report financial support was provided by UKRI. Luca Possidente and Fabio Freddi report a relationship with UK Research and Innovation that includes: funding grants. If there are other authors, they declare that they have no known competing financial interests or personal relationships that could have appeared to influence the work reported in this paper.

Data availability

Data will be made available on request.

Acknowledgements

This research is supported by the UK Research and Innovation Institution (UKRI) in the framework of the project RESTORE “Retrofit strategies for Existing STructures against prOgRessive collapse” (grant EP/X032469/1). Any opinions, findings, and conclusions or recommendations expressed in this paper are those of the authors and do not necessarily reflect the views of UKRI.

Nicola Tondini acknowledges the Italian Ministry of Education, Universities and Research (MUR), in the framework of the project DICAM-EXC (Departments of Excellence 2023-2027, grant L232/2016).

References

[1] J.M. Adam, F. Parisi, J. Sagaseta, X. Lu, Research and practice on progressive collapse and robustness of building structures in the 21st century, Eng. Struct. 173 (2018) 122–149.
[2] C. Pearson, N. Delatte, Ronan point apartment tower collapse and its effect on building codes, J. Perform. Constr. Facil 19 (2) (2005) 172–177.
[3] M.A. Sozen, C.H. Thornton, W.G. Corley, P.F. Mlakar, The Oklahoma City bombing: structure and mechanisms of the Murrah building, J. Perform. Constr. Facil 12 (3) (1998) 120–136.
[4] Z.P. Bazant, M. Verdure, Mechanics of progressive collapse: learning from world trade center and building demolitions, J. Eng. Mech. 133 (3) (2007) 308–319.
[5] X. Lu, H. Guan, H. Sun, Y. Li, Z. Zheng, Y. Fei, Z. Yang, L. Zuo, A preliminary analysis and discussion of the condominium building collapse in surfside, Florida, US, June 24, 2021, Front. Struct. Civ. Eng. 15 (2021) 1097–1110, https://doi.org/10.1007/s11709-021-0766-0.
[6] S. El-Tawil, H. Li, S. Kunnath, Computational simulation of gravity-induced progressive collapse of steel-frame buildings: current trends and future research needs, J Struct Eng (United States) 140 (8) (2014) 1–12.

[7] DOD (United States Department of Defense) (2016), Unified Facilities Criteria (UFC) – Design of Structures to Resist Progressive Collapse. 4–023-0314. July 2009 – Change 3, 1 November 2016, Arlington, Virginia.
[8] European Committee for Standardization (CEN) Eurocode 1, Actions on structures – Part 1–7: General actions – Accidental actions, European Standard EN 1991–1–7, Brussels, Belgium, 2006.
[9] GSA, 2003. Progressive Collapse Analysis and Design Guidelines for New Federal Office Buildings and Major Modernisation Projects, General Services Administration, Washington, DC.
[10] J.F. Demonceau, J.P. Jaspart, Experimental test simulating a column loss in a composite frame, Adv. Steel Constr. 6 (3) (2010) 891–913.
[11] G. Roverso, N. Baldassino, R. Zandonini, F. Freddi, Experimental assessment of an asymmetric steel-concrete frame under a column loss scenario, Eng. Struct. 293 (2023) 116610, https://doi.org/10.1016/j.engstruct.2023.116610.
[12] B. Yang, K.H. Tan, Experimental tests of different types of bolted steel beam column joints under a central column-removal scenario, Eng. Struct. 54 (2013) 112–130.
[13] C. Liu, K.H. Tan, T.C. Fung, Dynamic behaviour of web cleat connections subjected to sudden column removal scenario, J. Constr. Steel Res. 86 (2013) 92–106.
[14] H.Z. Jahromi, B.A. Izzuddin, D.A. Nethercot, S. Donahue, M. Hadjioannou, E.B. Williamson, M. Engelhardt, D. Stevens, K. Marchand, M. Waggoner, Robustness assessment of building structures under explosion, Buildings 2 (4) (2012) 497–518.
[15] R. Zandonini, N. Baldassino, F. Freddi, Robustness of steel-concrete flooring systems. An experimental assessment, Stahlbau 83 (9) (2014) 608–613.
[16] B.I. Song, Sezen, Experimental and analytical progressive collapse assessment of a steel frame building, Eng. Struct. 56 (2013) 664–672.
[17] H. Li, X. Cai, L. Zhang, B. Zhang, W. Wang, Progressive collapse of steel moment resisting frame subjected to loss of interior column: experimental tests, Eng. Struct. 150 (2017) 203–220.
[18] E.S. Johnson, J.E. Meissner, L.A. Fahnestock, Experimental behavior of a half-scale steel concrete composite floor system subjected to column removal scenarios, J. Struct. Eng. 142 (2) (2016) 1–12.
[19] N. Stathas, I. Karakasis, E. Strepelias, X. Palios, S. Bousias, M.N. Fardis, Tests and analysis of RC building, with or without masonry infills, for instant column loss, Eng. Struct. 193 (2019) 57–67.
[20] R. Zandonini, N. Baldassino, F. Freddi, G. Roverso, Steel-concrete composite frames under the column loss scenario: an experimental study, J. Constr. Steel Res. 162 (2019) 105527.
[21] T. Qu, B. Zeng, Z. Zhou, L. Huang, Failure mode discrimination and theoretical prediction method for unequal span bonded prestressed concrete substructures against progressive collapse, Eng. Fail. Anal. 156 (2024) 107839.
[22] M. D'Antimo, M. Latour, G. Rizzano, J.F. Demonceau, Experimental and numerical assessment of steel beams under impact loadings, J. Constr. Steel Res. 158 (2019) 230–247.
[23] F. Dinu, I. Marginean, D. Dubina, I. Petran, Experimental testing and numerical analysis of 3D steel frame system under column loss, Eng. Struct. 113 (2016) 59–70.
[24] F. Dinu, I. Marginean, D. Dubina, I. Petran, Experimental testing and numerical modelling of steel moment-frame connections under column loss, Eng. Struct. 151 (2017) 861–878.
[25] B.A. Izzuddin, A.G. Vlassis, A.Y. Elghazouli, D.A. Nethercot, Progressive collapse of multi-storey buildings due to sudden column loss — Part I: simplified assessment framework, Eng. Struct. 30 (2007) 1308–1318.
[26] A.G. Vlassis, B.A. Izzuddin, A.Y. Elghazouli, D.A. Nethercot, Progressive collapse of multi-storey buildings due to sudden column loss — Part II: application, Eng. Struct. 30 (2007) 1424–1438.
[27] G. Mucedero, E. Brunesi, F. Parisi, Nonlinear material modelling for fibre-based progressive collapse analysis of RC framed buildings, Eng. Fail. Anal. 118 (2020) 104901.
[28] M. Scalvenzi, S. Gargiulo, F. Freddi, F. Parisi, Impact of seismic retrofitting on progressive collapse resistance of RC frame structures, Eng. Fail. Anal. 131 (2022) 105840.
[29] F. Sadek, S. El-Tawil, H. Lew, Robustness of composite floor systems with shear connections: modeling, simulation, and evaluation, J. Struct. Eng. 134 (2008) 1717–1725.
[30] Y. Alashker, S. El-Tawil, F. Sadek, Progressive collapse resistance of steel–concrete composite floors, J. Struct. Eng. 136 (2010) 1187–1196.
[31] H.Z. Jahromi, A.G. Vlassis, B.A. Izzuddin, Modelling approaches for robustness assessment of multi-storey steel-composite buildings, Eng. Struct. 51 (2013) 278–294.
[32] S. Khan, S.K. Saha, V.A. Matsagar, B. Hoffmeister, Fragility of steel frame buildings under blast load, J. Perform. Constr. Facil. 31 (4) (2017) 04017019.
[33] D. Stephen, D. Lam, J. Forth, J. Ye, K.D. Tsavdaridis, An evaluation of modelling approaches and column removal time on progressive collapse of building, J. Constr. Steel Res. 153 (2019) 243–253.
[34] C. Dimopoulos, F. Freddi, T.L. Karavasilis, G. Vasdravellis, Progressive collapse of self-centering moment resisting frames, Eng. Struct. 208 (2020) 109923.
[35] F. Parisi, M. Scalvenzi, Progressive collapse assessment of gravity-load designed European RC buildings under multi-column loss scenarios, Eng. Struct. 209 (2020) 110001.
[36] F. Freddi, L. Ciman, N. Tondini, Retrofit of existing steel structures against progressive collapse through roof-truss, J. Constr. Steel Res. 188 (2022) 107037.
[37] S. Mazzoni, F. McKenna, M.H. Scott, G.L. Fenves, Open System for Earthquake Engineering Simulation User Command-Language Manual, OpenSees Version 2.0, University of California, Berkeley, CA, 2009.
[38] J.-M. Franssen, T. Gernay, Modeling structures in fire with SAFIR®: theoretical background and capabilities, J. Struct. Fire Eng. 8 (3) (2017) 300–323.
[39] ABAQUS, ABAQUS Version 6.14, User's Manual, Dassault 618 Systèmes, Vélizy-Villacoublay, France, 2014.
[40] ANSYS Inc, ANSYS versrefboion 17.0, User's Manual, ANSYS, Canonsburg, PA, 2016.
[41] DIANA FEA BV, DIANA Version 10.1, User's Manual, DIANA FEA BV, Delft, Netherlands, 2016.
[42] L. Possidente, N. Tondini, J.-M. Battini, Branch-switching procedure for post-buckling analyses of thin-walled steel members in fire, Thin-Walled Struct. 136 (2019) 90–98.
[43] L. Possidente, N. Tondini, J.-M. Battini, 3D beam element for the analysis of torsional problems of steel-structures in fire, J. Struct. Eng. 146 (7) (2020).
[44] P.A. Heng, J.-M. Battini, M. Hjiaj, Co-rotating rigid beam with generalized plastic hinges for the non-linear dynamic analysis of planar framed structures subjected to impact loading, Finite Elem. Anal. Des. 157 (2019) 38–49.
[45] G. Kaewkulchai, E.B. Williamson, Beam element formulation and solution procedure for dynamic progressive collapse analysis, Comput. Struct. 82 (7–8) (2004) 639–651.
[46] F. Parisi, N. Augenti, Influence of seismic design criteria on blast resistance of RC framed buildings: a case study, Eng. Struct. 44 (2012) 78–93.
[47] L. Possidente, A. Weiss, D. de Silva, S. Pustorino, E. Nigro, N. Tondini, Fire safety engineering principles applied to a multi-storey steel building, Proc. Inst. Civ. Eng. – Struct. Build. 174 (9) (2021) 725–738.
[48] S. Gerasimidis, C. Bisbos, C. Baniotopoulos, Vertical geometric irregularity assessment of steel frames on robustness and disproportionate collapse, J. Constr. Steel Res. 74 (2012) 76–89.
[49] S. Gerasimidis, Analytical assessment of steel frames progressive collapse vulnerability to corner column loss, J. Constr. Steel Res. 95 (2014) 1–9.
[50] T. Gernay, A. Gamba, Progressive collapse triggered by fire induced column loss: detrimental effect of thermal forces, Eng. Struct. 172 (2018) 483–496.
[51] A.K. Chopra, Dynamics of Structures: Theory and Applications to Earthquake Engineering, Prentice-Hall, New Jersey, 1995.
[52] U. Starrossek, Typology of progressive collapse, Eng. Struct. 29 (9) (2007).
[53] D.J. Stevens, B. Crowder, B. Hall, K. Marchand, Unified Progressive Collapse Design Requirements for DoD and GSA, Structures Congress, Vancouver Canada, April 2008.
[54] J. Mashhadi, H. Saffari, Effects of damping ratio on dynamic increase factor in progressive collapse, Steel Comps. Struct. 22 (3) (2016) 677–690.
[55] M. Liu, A new dynamic increase factor for non-linear static alternate path analysis of building frames against progressive collapse, Eng. Struct. 48 (2013) 666–673.

[56] M.H. Tsai, B.H. Lin, Dynamic amplification factor for progressive collapse resistance analysis of a RC building, Struct. Des. Tall Spec. Build. 18 (5) (2009) 539–557.
[57] J. Mashhadi, H. Saffari, Modification of dynamic increase factor to assess progressive collapse potential of structures, J. Constr. Steel Res. 138 (2017) 72–78.
[58] M.H. Tsai, An analytical methodology for the dynamic amplification factor in progressive collapse evaluation of building structures, Mech. Res. Commun. 37 (2010) 61–66.
[59] M. Ferraioli, A modal pushdown procedure for progressive collapse analysis of steel frame structures, J. Constr. Steel Res. 156 (2019) 227–241.
[60] E. Brunesi, F. Parisi, Progressive collapse fragility models of European reinforced concrete framed buildings based on pushdown analysis, Eng. Struct. 152 (2017) 579–596.
[61] H. Elsanadedy, H. Sezen, H. Abbas, T. Almusallam, Y. Al-Salloum, Progressive collapse risk of steel framed building considering column buckling, Eng. Sci. Technol. Int. J. 35 (2022) 101193.
[62] CEN (European Committee for Standardization), Eurocode 1: Actions on structures – Part 1–1: General actions - densities, self-weight, imposed loads for buildings, EN 1991-1-1, Brussels, Belgium, 2002.
[63] CEN (European Committee for Standardization), Eurocode 3: Design of steel structures – Part 1–1: General rules and rules for building, EN 1993–1–1. Brussels, Belgium, 2005.
[64] CEN (European Committee for Standardization), Eurocode 8: Design of Structures for Earthquake Resistance. Part 1: General Rules, Seismic Action and Rules for Buildings, EN 1998–1, Brussels, Belgium, 2005.
[65] J. Jönsson, T.-C. Stan, European column buckling curves and finite element modelling including high strength steels, J. Constr. Steel Res. 128 (2017) 136–151.
[66] L. Possidente, N. Tondini, J.-M. Battini, Torsional and flexural-torsional buckling of compressed steel members in fire, J. Constr. Steel Res. 171 (2020) 106130.
[67] CEN (European Committee for Standardization), Eurocode 3: Design of steel structures – Part 1–1: General rules and rules for buildings, ENV 1993–1–1, Brussels, Belgium, 2004.
[68] C.-H. Lee, S. Kim, K. Lee, Parallel axial-flexural hinge model for non linear dynamic progressive collapse analysis of welded steel moment frames, J. Struct. Eng. 136 (2) (2009) 165–173.
[69] J.M. Castro, A.Y. Elghazouli, B.A. Izzuddin, Modelling of the panel zone in steel and composite moment frames, Eng. Struct. 27 (2005) 129–144.
[70] F.A. Charney, W.M. Downs, Modeling procedures for panel zone deformations in moment resisting frames, in: Proc. Conference on Connections in Steel Structures V: Innovative Steel Connections, Amsterdam, the Netherlands, 2004.